ID 3889

Agip S.p.A.

STAT

Direzione Staff Tecnico

GEDA

Studi di Geodinamica e dell'Ambiente

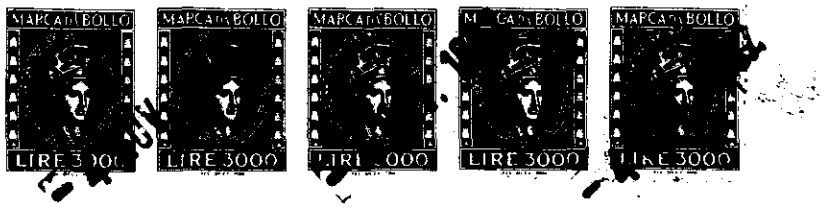

PREVISIONI PRELIMINARI DI SUBSIDENZA

per il Campo di BOMBA

Nota tecnica

Data 6 marzo 1989

Relazione n° 1372 (aggiornamento della rel.n. 1170)

Autori:

E. Norelli E Norelli

C. Zoccatelli

visto
Il Responsabile
Dr G. Dossena

Inviato a:

VGI - Ing. Vaghi

VTE - Ing. Henking

e p.c. SIAT - Ing. Rogialli

PREVISIONE DELLA SUBSIDENZA

PER IL CAMPO DI BOMBA

Questo documento rappresenta l'aggiornamento della relazione GEDA n.1170 del 31/12/87.

Tale aggiornamento si e` reso necessario in seguito all'acquisizione di nuovi dati sperimentali relativi alle proprieta` petrofisiche della roccia serbatoio, in modo particolare in relazione ai coefficienti di compressibilita' uniassiale.

1) generalita`

Per le caratteristiche giacimentologiche, geologiche e geometriche, per i piani di sviluppo e le previsioni di comportamento dinamico, si e` fatto riferimento alla

documentazione GIAC 1970-77.

Il reservoir si sviluppa su un'area di circa 7,8 [km2] in calcari miocenici e cretacei con top compreso fra 1236 e 1388 [m] dal p.c. con un gross pay massimo di 126 [m] circa.

Ha forma ellittica con diametro maggiore di 3 [km] e minore di 2 (all. 3).

La struttura è una piega anticlinale con fianco ribassato per faglia, come evidenziato dalla sezione schematica ENE-OSO dell'allegato 13.

Sono state individuate dall'alto verso il basso due zone con caratteristiche petrofisiche buone nella superiore e piu` scadenti in quella inferiore:

Zona A

porosita` media	6,6	[%]
saturazione in acqua	10	[%]
permeabilita` media	13	[md]
GOIP	2.000.000.000	[Nm3]
net bulk volume	237.000.000	[m3]

Zona B

porosita` media	7,4	[%]
saturazione in acqua	20	[%]

permeabilita` media	3,4	[md]
GOIP	1.250.000.000	[Nm3]
net bulk volume	148.660.000	[m3]

2) parametri di base per il colcolo

Si e` considerata una produzione totale prevista di circa 1.500.000.000 [Nm3] nell'arco di venti anni (allegato 16), il che comporterebbe, secondo i tassi di estrazione annuali previsti, un decremento finale di pressione di circa 30 [kg/cm2] a partire da una pressione statica iniziale di giacimento di 141.6 [kg/cm2] @ 1060 [mlm]

Il valore del gradiente di overburden (stimato da un campo con caratteristiche litologiche analoghe) si aggira intorno a 0.2059 [atm/m] @ 1450 [mtr] con conseguente pressione di overburden di 298 [kg/cm2] e quindi con una pressione effettiva iniziale di 156 [kg/cm2].

3) coefficiente di compressibilita` uniassiale Cm

Da una ricerca bibliografica su dati sperimentali di

compressibilita` uniassiale relativi a rocce calcaree, sono stati tratti i diagrammi illustrati sugli allegati 6, 7, 8, e 9.

Alle pressioni effettive o alle porosita` corrispondenti il range dei valori di Cm (calcolato in due casi da Cp) varia da 2 a 8 * 10-6 [cm2/kg].

L'allegato 10 fa riferimento a dei test di deformazione fino a rottura condotti su calcari per varie pressioni di confinamento e per varie velocita` di incremento del carico assiale.

Gli allegati 11 e 12 riportano i valori di Cm ottenuti da test di laboratorio eseguiti direttamente su carote prelevate dai livelli produttivi del campo.

I valori di allegato 11 derivano da test di tipo triassiale ed edometrico recentemente condotti da Agip/Lapr, mentre la curva di allegato 12 e` stata estrapolata dalla media dei valori ricavati da 18 test di comprimibilita` dei pori in cella idrostatica da Agip/Chimfi (1977).

Per valori di pressione effettiva attorno a 100 [kg/cm2] i dati sono confrontabili; a pressioni superiori i test in cella idrostatica danno dei risultati piu` elevati

per circa un ordine di grandezza, quelli triassiali ed edometrici si allineano invece con i dati riportati dalla letteratura.

Per il calcolo della compattazione il valore di Cm piu` adeguato, tenuto conto soprattutto dei test condotti in Agip e dell'opportunita` di privilegiare in questo tipo di elaborazione i valori piu` conservativi, e` stato individuato in 0,000013446 [cm2/kg] @ 156 [kg/cm2] di pressione effettiva.

4) calcolo della subsidenza

La metodologia generale seguita per la definizione del problema e` illustrata dallo schema di allegato 2.

Il modello utilizzato per il calcolo e` quello di GEERTSMA a nuclei di deformazione, modificato da Puppi et al. (Universita` di Bologna 1984-85).

Tale modello prevede la scomposizione del giacimento in celle elementari, di ognuna delle quali viene fornito spessore e profondita` dal piano campagna; gli allegati 3, 4 e 5 riportano le mappe che sono servite per il calcolo dei

parametri delle cellette e sono rispettivamente: mappa delle isobate del top del reservoir, mappa delle isopache della copertura e mappa del gross pay.

I dati completi di input del modello sono riportati in allegato 15.

I risultati sono illustrati in allegato 14, sul quale sono tracciate le curve di ugual subsidenza che danno un valore massimo, in corrispondenza del centro del reservoir, di circa 1,5 [cm].

In corrispondenza della diga il cedimento calcolato e' di 1.0 [cm].

Da notare che, nell'ipotesi di alimentazione dell'acquifero di fondo da parte del bacino idrografico della Maiella (sezione schematica allegato 13), ipotesi abbastanza realistica considerando la bassissima salinita' dell'acquifero di fondo e la sovrapressione del gas in giacimento, il decremento massimo di pressione nei livelli produttivi potrebbe ridursi a qualche [kg/cm2], riducendo cosi' proporzionalmente il valore della subsidenza massima a qualche millimetro.

Si segnalano infine, in quanto strettamente connessi

con la problematica della subsidenza, due recenti elaborati: "Studio fotogeologico sulla stabilita` dei varsanti dell'area limitrofa al giacimento di Bomba (a cura di SEPI/FOIN Marzo/1987) e "Rapporto sul rilievo planoaltimetrico e livellazione geometrica di precisione per il controllo dei movimenti del suolo, eseguiti nella zona di Bomba (Chieti) nel corso del 1988 (OPSI/GEOD).

BIBLIOGRAFIA

1) **HALL, H. N.** - "Compressibility of reservoir rocks" Trans. AIME (1953) 198-309.

2) **SHREINER L. A., BAYDYUK B. V, & PAVLOVA N. N.** - "Deformational properties of rocks as applied to petroleum geology and deep hole drilling" 7th World Petr. Cong. - Mexico City.

3) **GEERTSMA,J.**;1973 - Land Subsidence Above Compacting Oil and Gas Reservoirs. SPE AIME.

4) **TEEUW,D.**;1971, - Prediction of Formation Compaction from Laboratory Compressibility Data : S.P.E. Journal, Vol. 11 - n. 5.

5) **CHILINGAR,G.V et alii**;1982 - Compressibilities of Sands and Clays : Proceedings of 1982 Forum on Subsidence Due to Fluid Withdrawls, Checotah, Oklahoma.

- 4 NOV. 1982

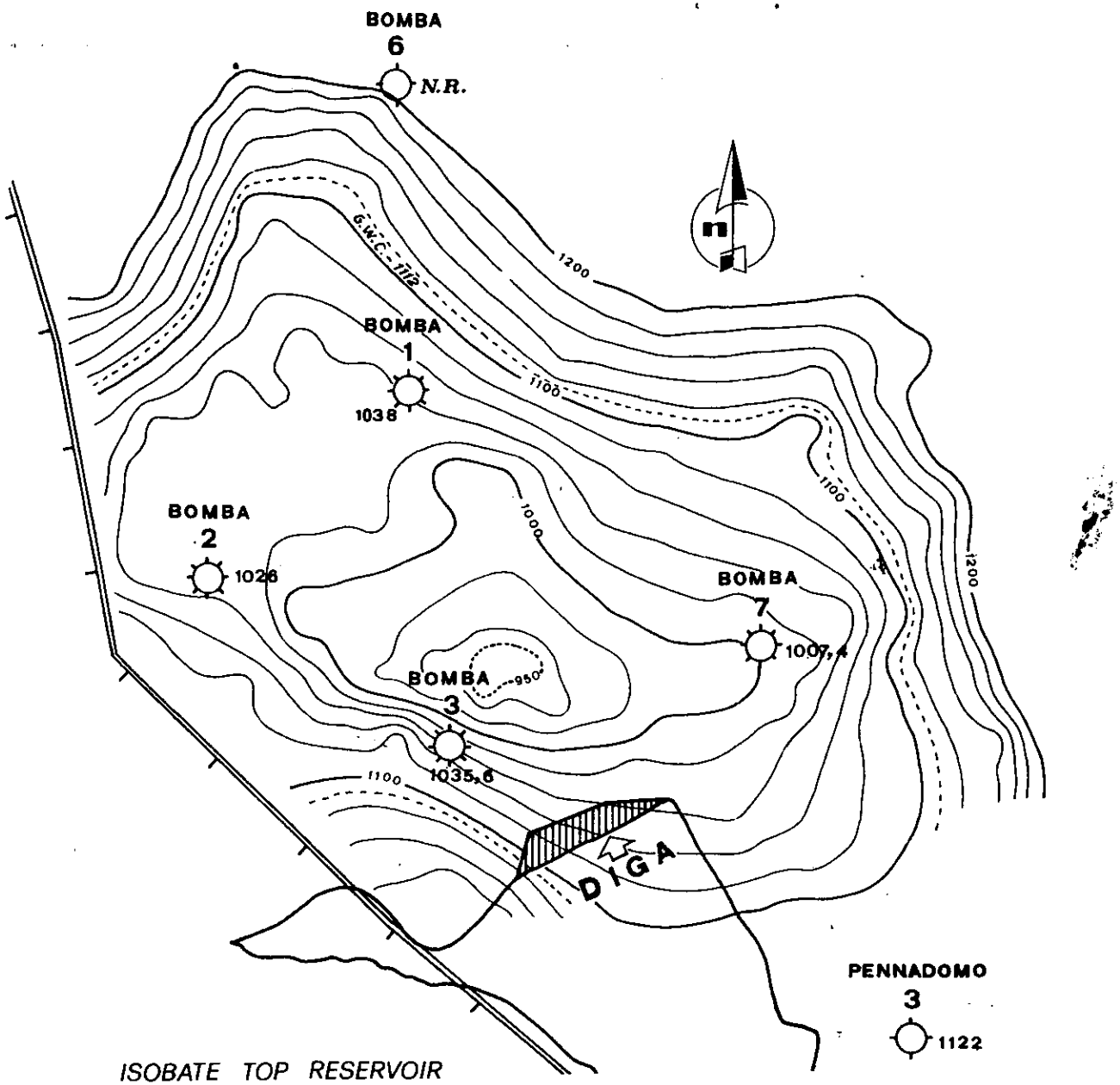

ISOBATE TOP RESERVOIR

(Elaborazione da mappa GIAC, 1977)

SCALA 1:25000

Agip

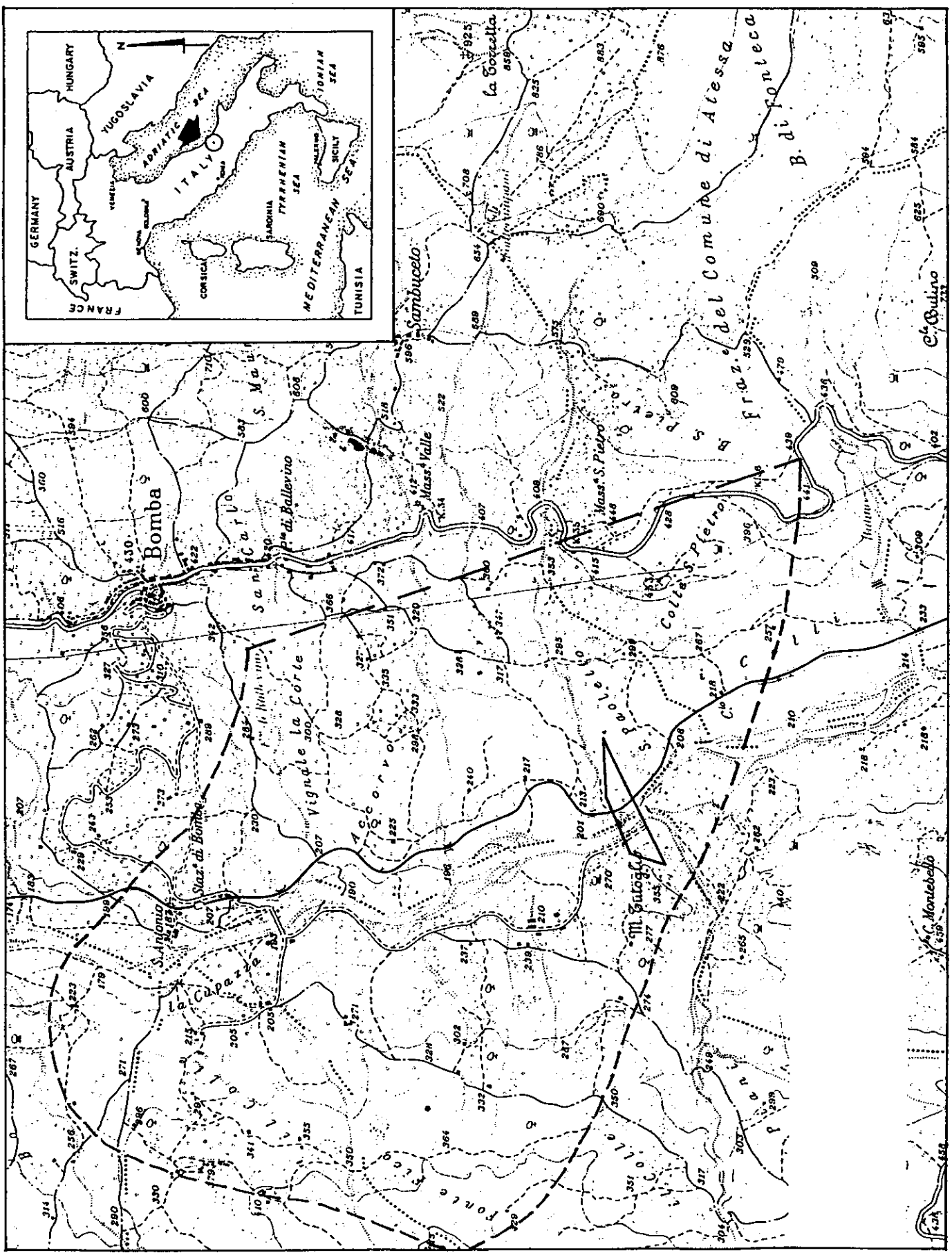

Agip

Allegato 1

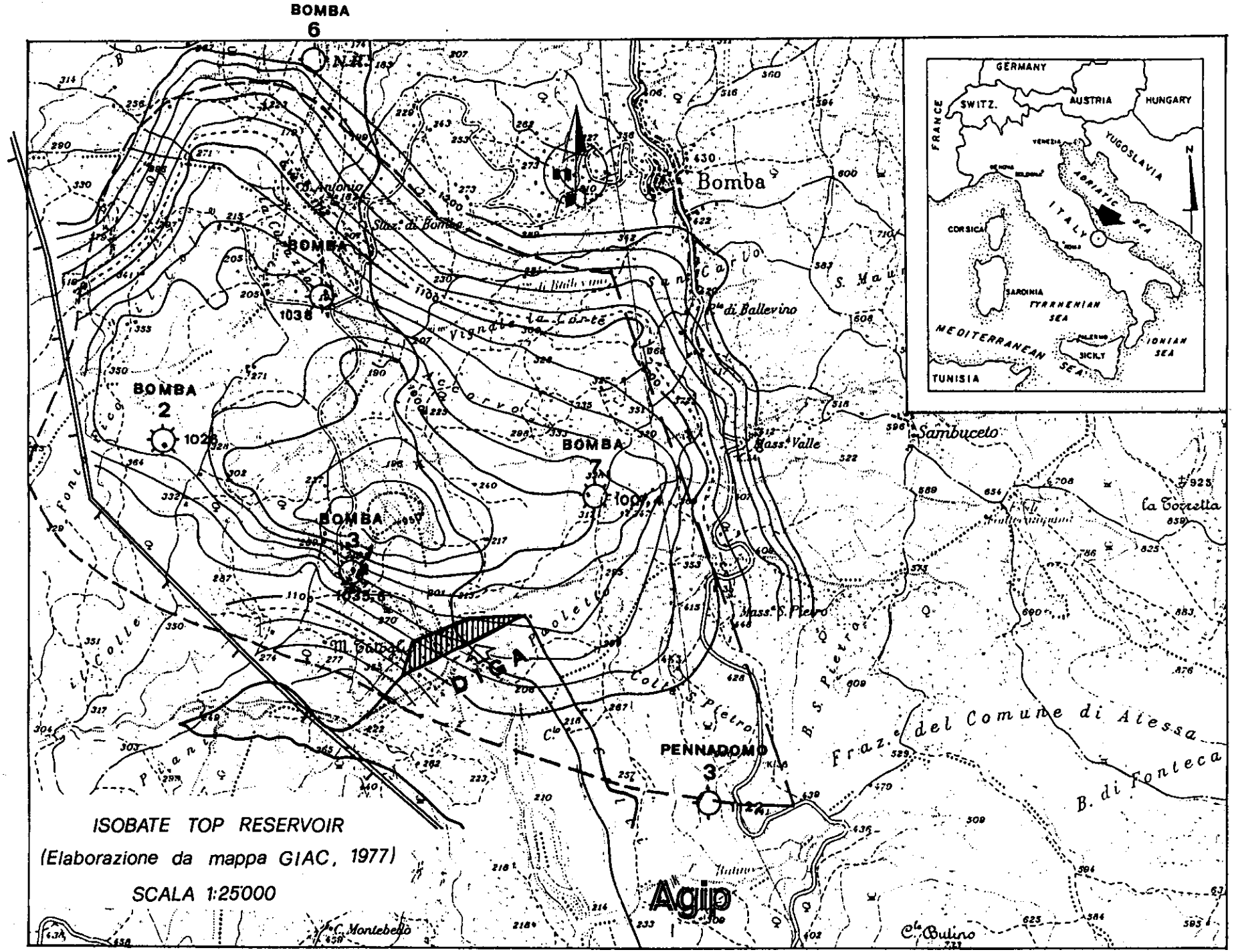

Agip

AGIP Spa — GEDA/GEDI

Allegato 1

Allegato 2

CAMPO DI BOMBA – ISOPACA DELLA COPERTURA
(p.c. ÷ TOP RES)

SCALA 1:25'000

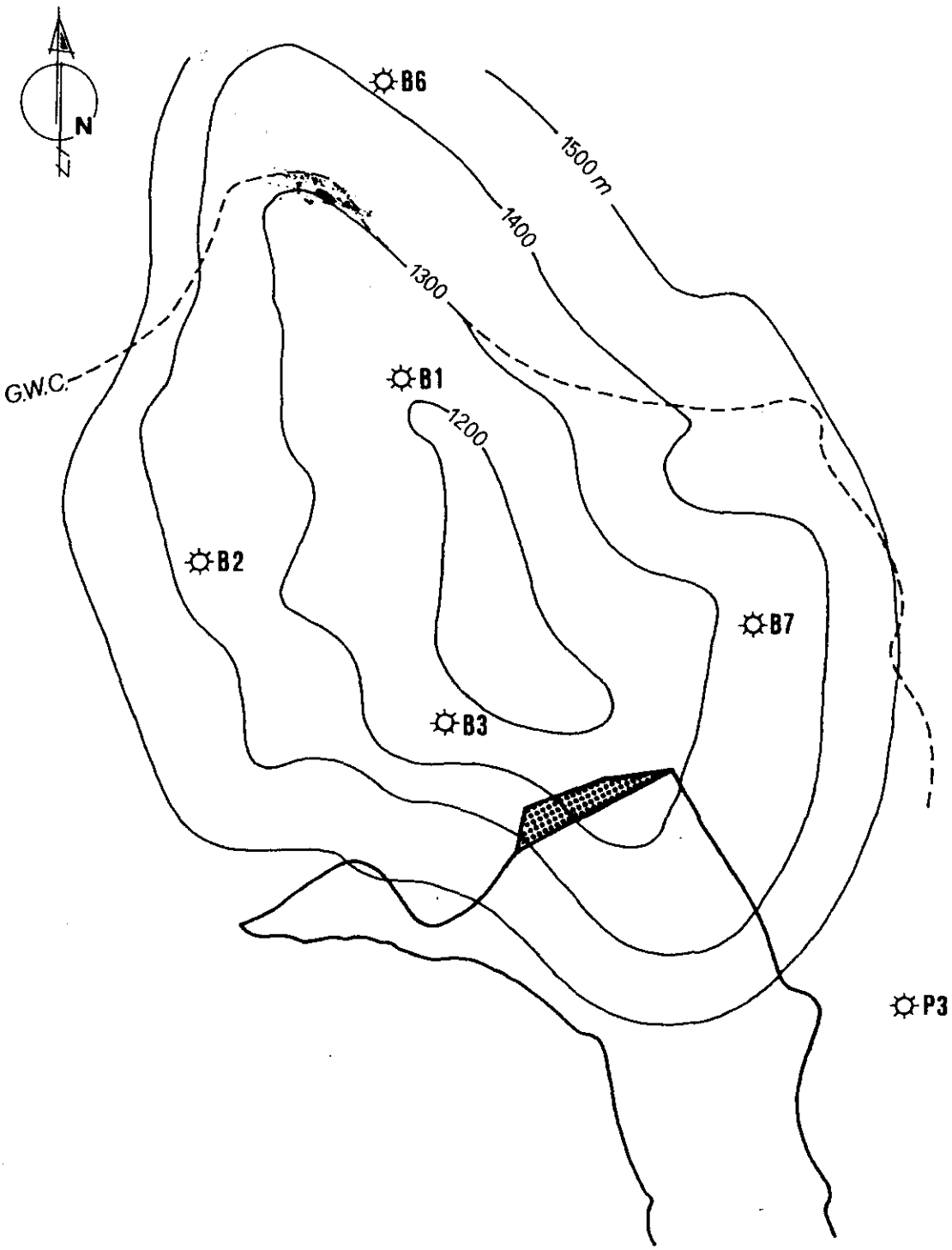

N
SCOMPOSIZIONE GEOMETRICA DEL RESERVOIR
42 ISOPACHE DEL RESERVOIR (in metri)
G.W.C.
7 POZZI
DIGA
FAGLIA
0
0.5
1 km
AGIP Spa
GEDA/GEDI

Uniaxial compaction coefficient c_m (vertical axes) for carbonate rock. Effective vertical stress range $\sigma_z = 100-200\ kg/cm^2$ corresponding to depth of burial of 1000 m for normally pressured reservoirs

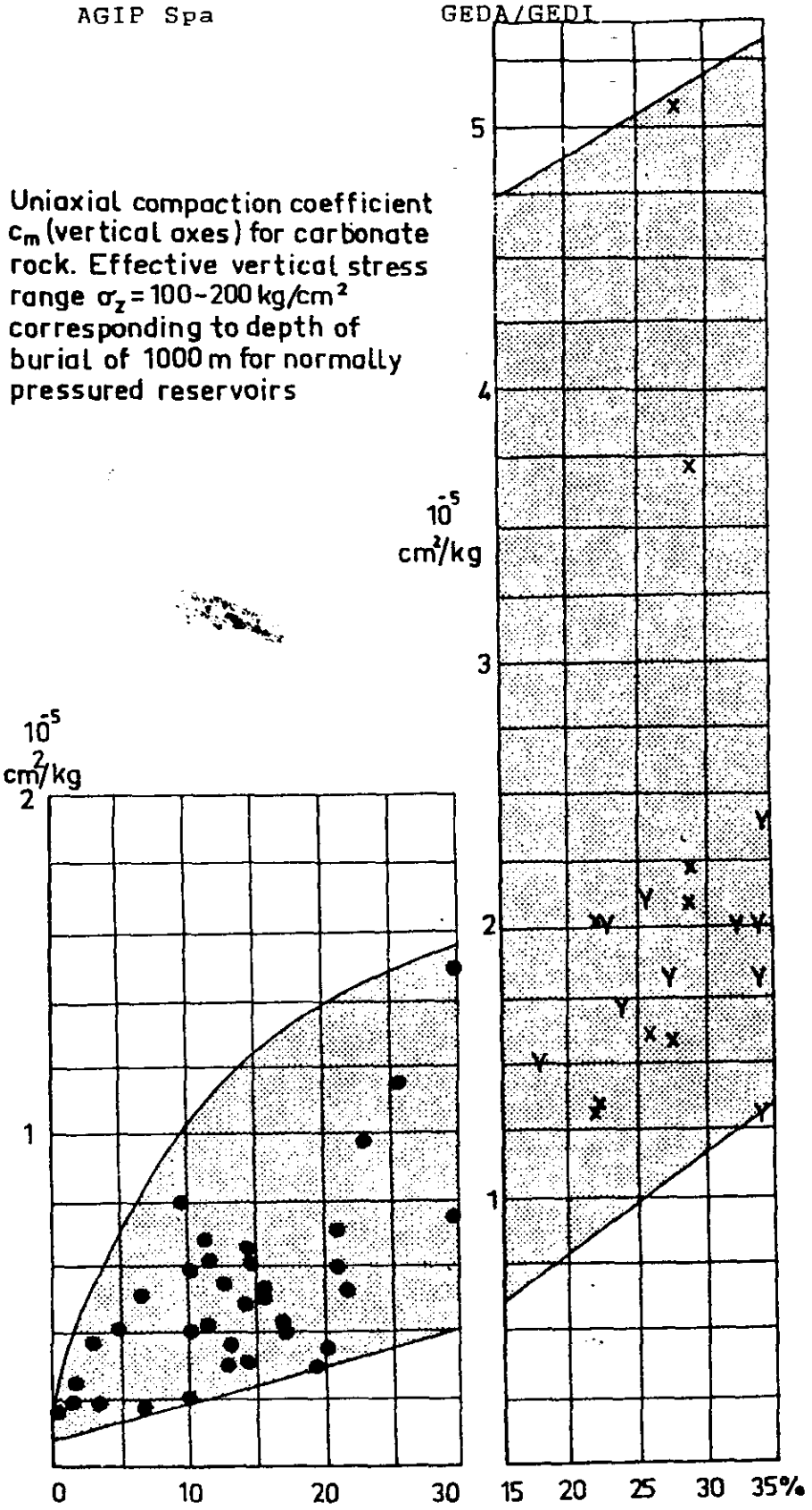

Well - consolidated

Vuggy carbonate x
Soft limestone Y

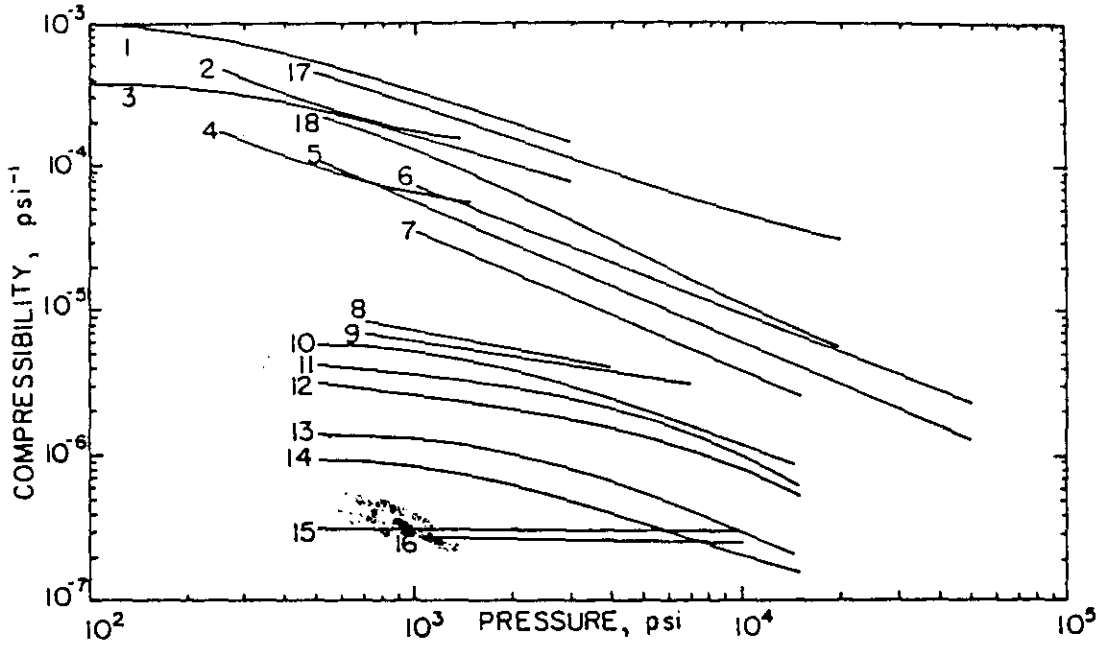

—Relationship between compressibility (psi^{-1}) and applied pressure (psi) for unconsolidated sands, illite clay, limestone, sandstones and shale.

No.	Investigator	Rock type	Type of applied pressure		Compressibility
1	The writers	California unconsolidated arkosic sands*	Hydrostatic	Pore	$[-(1/V_p)(\partial V_p/\partial p_e)_\sigma]$
2	Kohlhaas and Miller (1969)	California unconsolidated sands	Uniaxial	Pore	
3	The writers	California unconsolidated arkosic sands*	Hydrostatic	Bulk	$[-(1/V_b)(\partial V_b/\partial p_e)_\sigma]$
4	Kohlhaas and Miller (1969)	California unconsolidated sands	Uniaxial	Bulk	
5	The writers	Illite clay (API No. 35) (wet)**	Uniaxial	Bulk	$[-(1/e+1)(de/dp_{ei})]$
6	The writers	Illite clay (API No. 35) (dry)	Uniaxial	Bulk	$[-(1/h)(dh/dp_e)]$
7	Knutson and Bohor (1963)	Repetto Fm. (Grubb Zone) (wet)*	Net confining	Pore	$[-(1/V_p)(\partial V_p/\partial\sigma)_{p_p}]$
8	Knutson and Bohor (1963)	Lansing-Kansas City Limestone (wet)*	Net confining	Pore	
9	Carpenter and Spencer (1940)	Woodbine Sandstone (wet)	Net confining	Pseudo bulk	$[-(1/V_b)(\partial V_p/\partial p)]$
10	Fatt (1958b)	Feldspathic graywacke (No. 10) (wet)***	Net confining****	Bulk	
11	Fatt (1958b)	Graywacke (No. 7) (wet)***	Net confining	Bulk	
12	Fatt (1958b)	Feldspathic graywacke (No. 11) (wet)***	Net confining	Bulk	
13	Fatt (1958b)	Lithic graywacke (No. 12) (wet)***	Net confining	Bulk	$[-(1/V_b)(\partial V_b/\partial p_t)_{p_p}]$
14	Fatt (1958b)	Feldspathic quartzite (No. 20) (wet)***	Net confining	Bulk	
15	Podio et al. (1968)	Green River shale (dry)	Net confining	Bulk	
16	Podio et al. (1968)	Green River shale (wet)**	Net confining	Bulk	
17	Chilingarian et al. (1973)	Montmorillonite clay saturated in sea water	Hydrostatic		$c_b = -\frac{1}{V_b}\left(\frac{\partial V_b}{\partial p_e}\right)_{\sigma,T}$
18	Chilingarian et al. (1973)	Montmorillonite clay saturated in sea water	Uniaxial		$c_b = -\frac{1}{h}\left(\frac{\partial h}{\partial p}\right)$

*Saturated with formation water.
**Saturated with distilled water.
***Saturated with kerosene.
****Net confining pressure = external hydrostatic pressure on a jacketed specimen = $p_e = (\sigma - 0.85p_p)$, where σ is the total overburden stress and p_p is the pore pressure. Stresses in the triaxial apparatus of Sawabini et al. (1971) approached hydrostatic; i.e., three principal stresses in x, y and z directions are equal.

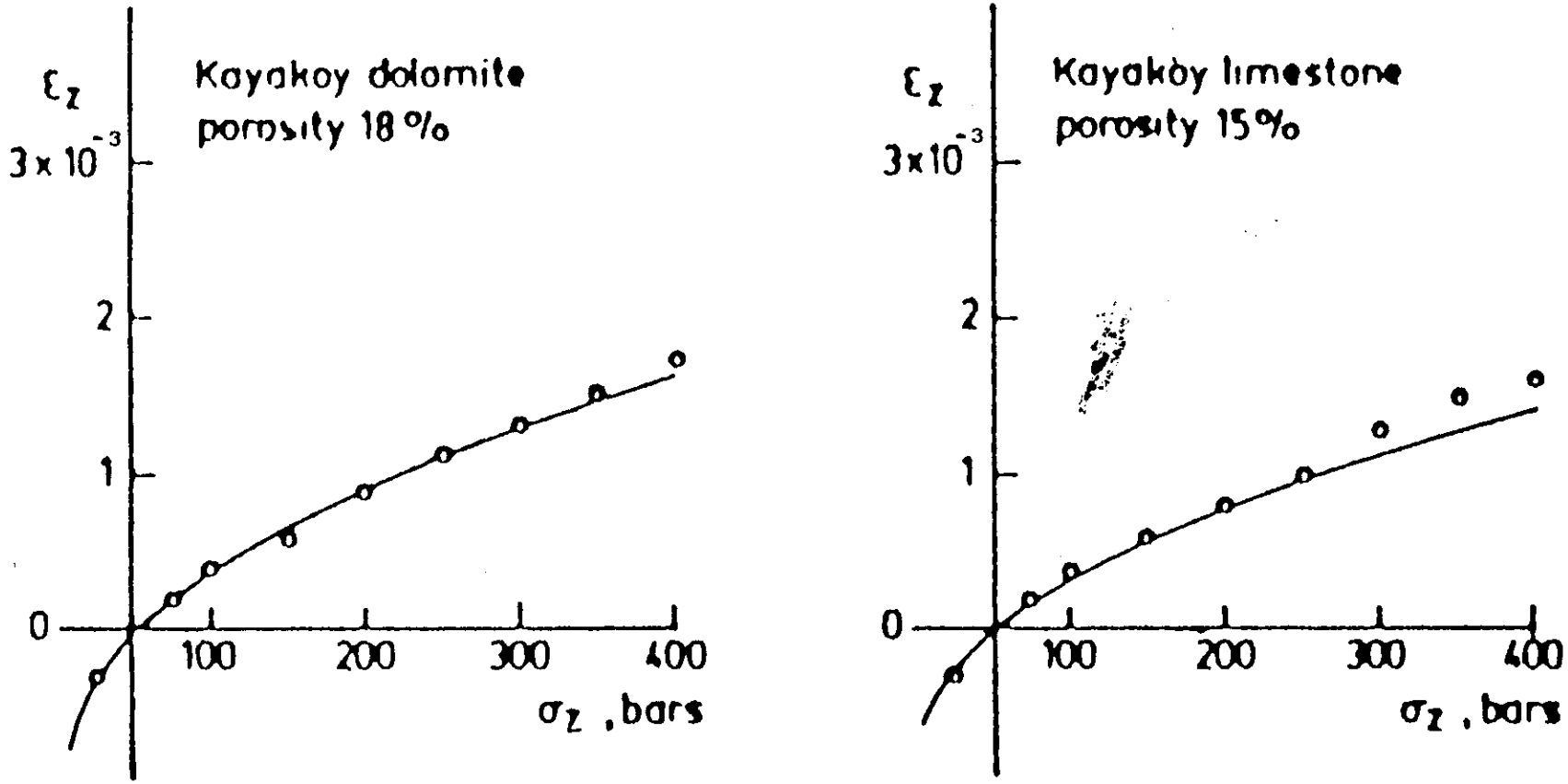

COMPARISON OF UNIAXIAL COMPACTIONS DERIVED FROM HYDROSTATIC DATA (CURVES) AND OBTAINED IN OEDOMETER TESTS (DOTS) FOR KAYAKOEY CARBONATE ROCKS.

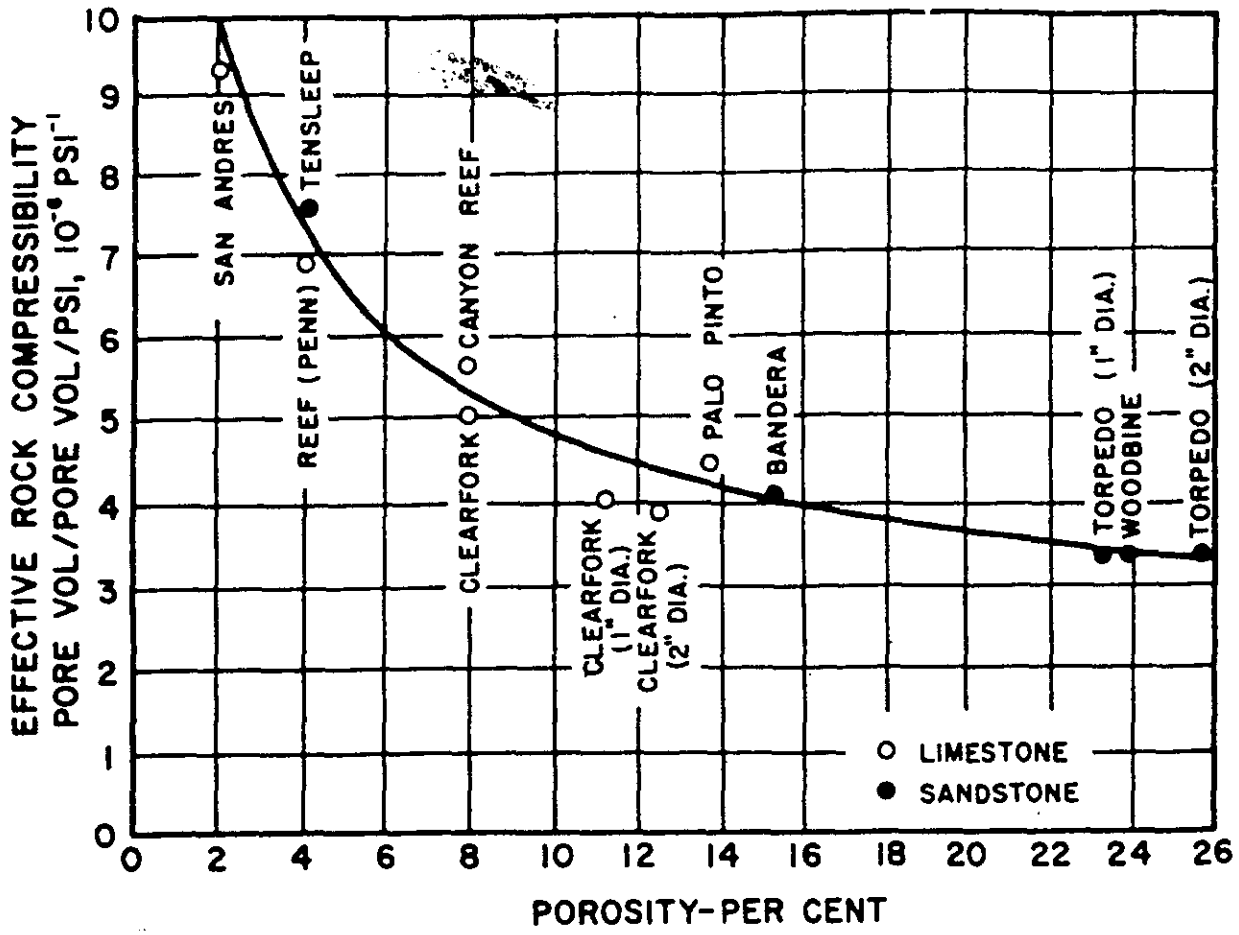

Effective formation compressibility versus porosity. (Hall, *Trans.* AIME)

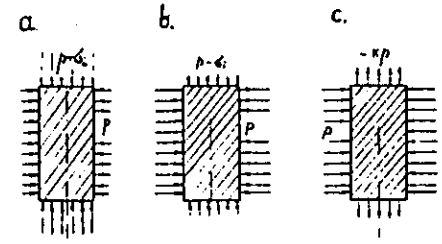

$$\sigma_i = \frac{1}{\sqrt{2}}\sqrt{(\sigma_1-\sigma_2)^2+(\sigma_2-\sigma_3)^2+(\sigma_3-\sigma_1)^2}$$

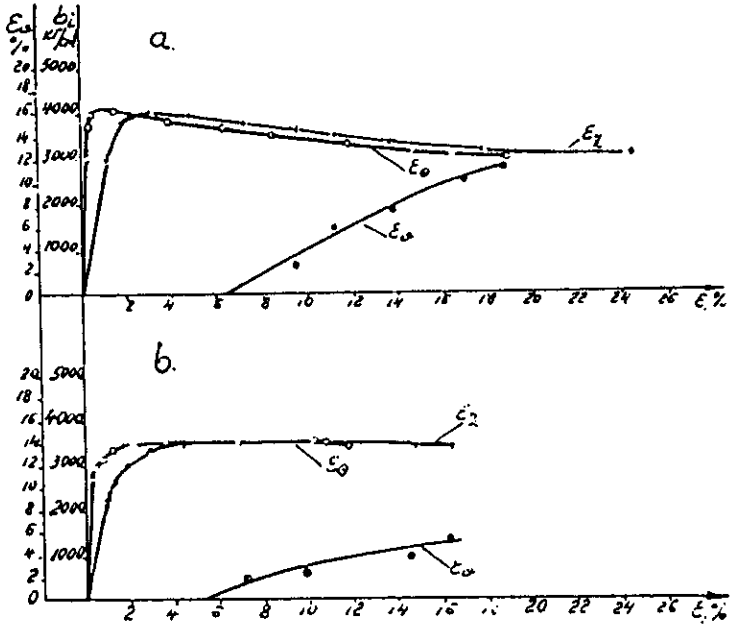

Diagrams of limestone deformation (homogeneous, fine-grained, grain size 0,01–0,04 mm) at longitudinal loading rates a) $\frac{\Delta\sigma_i}{\Delta t}$ = 500 kg/cm/sec, b) $\frac{\Delta\sigma_i}{\Delta t}$ = 0,1 kg/cm/sec. under confining pressure, p = 1000 kg/cm at first loading scheme;

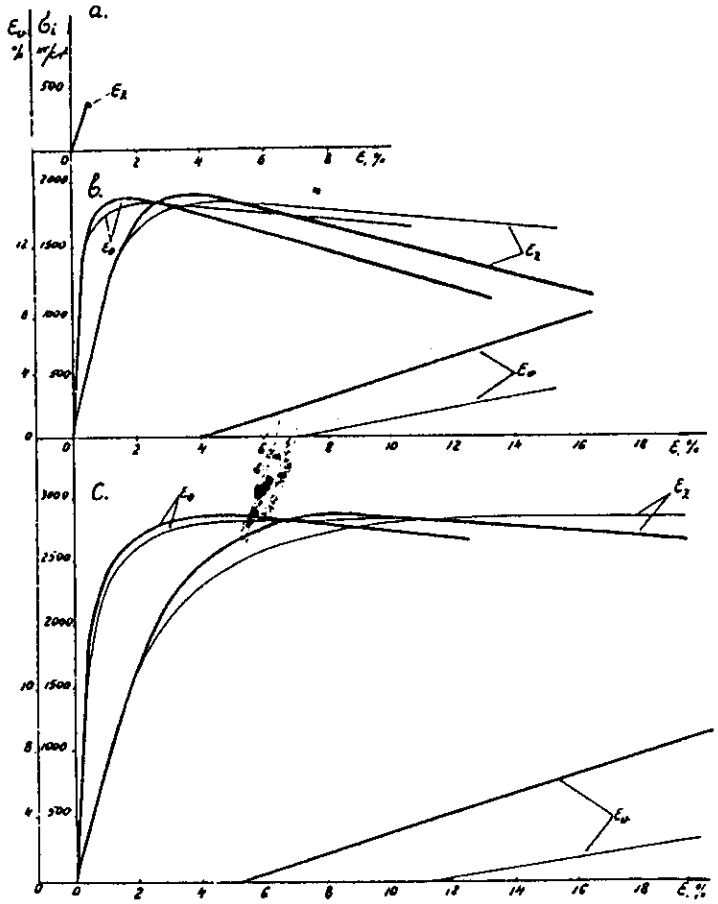

Diagrams of limestone deformation (of organic-detritus type with clay 10–15% and quartz 2–3% impurities). At first loading scheme under confining pressure and temperature: a) p = 1 kg/cm, t = 20 C; b) p = 750 kg/cm, t = 100 C; c) p = 1500 kg/cm, t = 200 C. Thick lines — at 20 C;

ε_z = linear lengthwise strain; ε_0 = lateral strain; ε_v = relative increase of volume (decompaction at strain)

-BOMBA 3- COEFF. Cb - Cm

CAROTA DA/A CAMPIONE N.	LITOTIPO ETA'	Cb cm2/kg	Cm cm2/kg
1238.5-1247.5 420	CALCARE ORGANOGENO	5.80*10-6	4.02*10-6
1247.5-1256.5 468*	CALCARE ORGANOGENO	---------	---------
1256.5-1265.5 614	CALCARE ORGANOGENO	6.44*10-6	4.36*10-6
1292.5-1301.5 920	CALCARE BIANACSTRO	7.46*10-6	4.72*10-6
1301.5-1307 1013	CALCARE BIANCASTRO	5.02*10-6	2.98*10-6

* Valori mancanti causa cattivo funzionamento Strain gage.

-BOMBA 3- COEFF. DI COMPATTAZIONE

CAROTA DA/A CAMPIONE N.	LITOTIPO ETA'	SIGMA 1 kg/cm2	Cm cm2/kg
1238.5-1247.5 420	CALCARE ORGANOGENO	100	5.32*10-6
		200	3.93*10-6
		300	4.11*10-6
1247.5-1256.5 468	CALCARE ORGANOGENO	100	8.82*10-6
		200	4.83*10-6
		300	3.74*10-6
1256.5-1265.5 614	CALCARE ORGANOGENO	100	1.39*10-5
		200	7.66*10-6
		300	5.36*10-6
1292.5-1301.5 920	CALCARE BIANACSTRO	100	1.66*10-5
		200	7.38*10-6
		300	4.89*10-6
1301.5-1307 1013	CALCARE BIANCASTRO	100	1.48*10-5
		200	5.86*10-6
		300	4.43*10-6

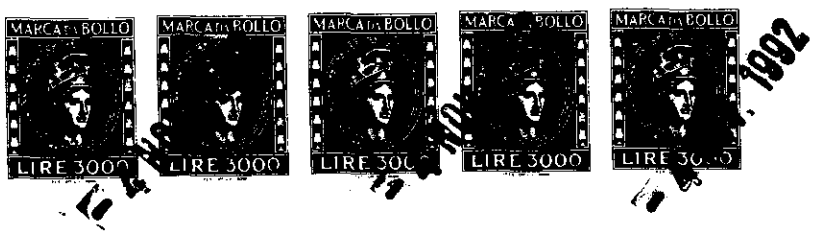

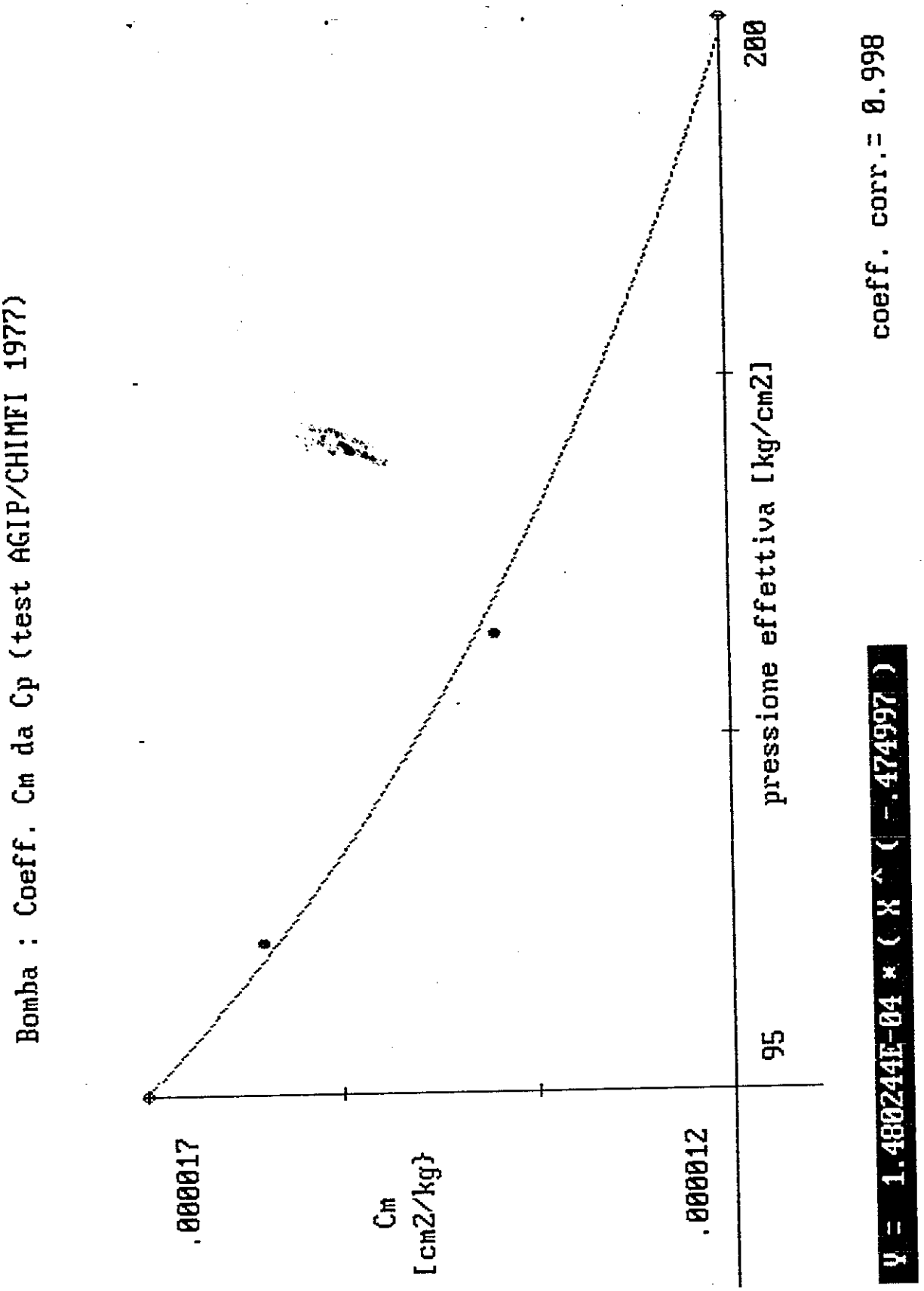
Bomba : Coeff. Cm da Cp (test AGIP/CHIMFI 1977)
.000017
Cm
[cm2/kg]
.000012
95
pressione effettiva [kg/cm2]
200
coeff. corr.= 0.998
Y = 1.480244E-04 * (X ^ (-.474997)

CAMPO DI BOMBA

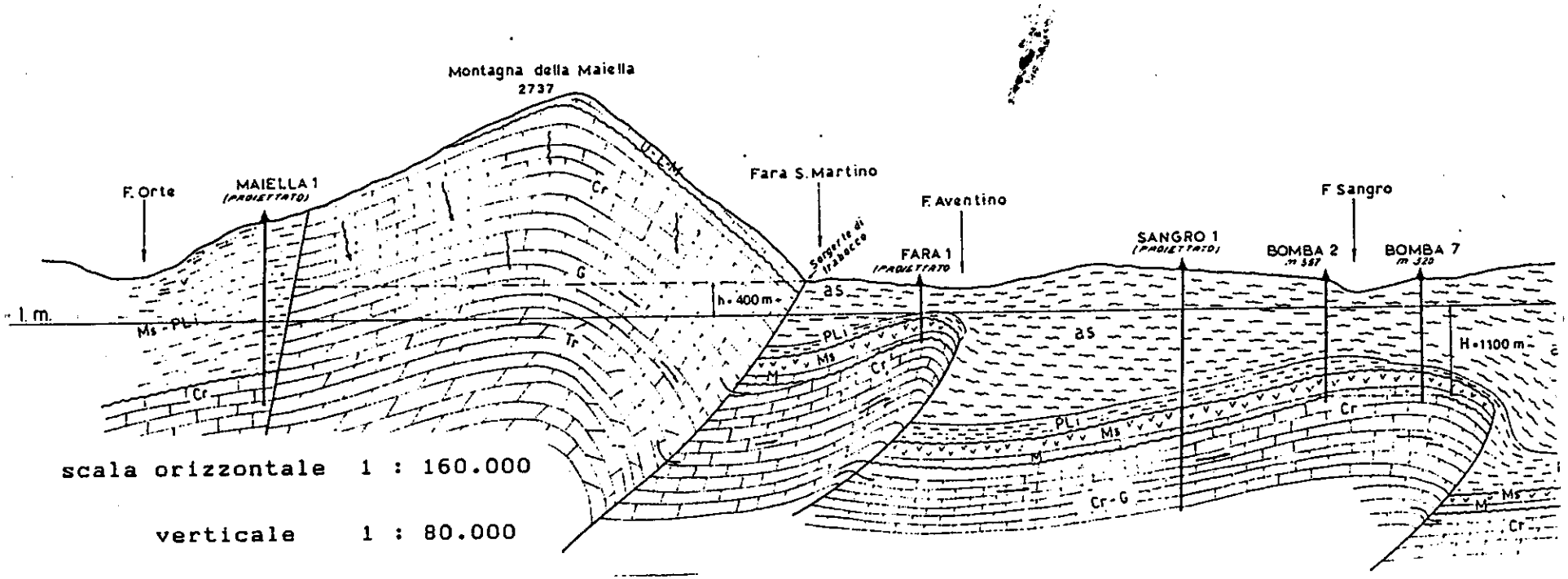

scala orizzontale 1 : 160.000

verticale 1 : 80.000

aS = *Terreni sciolti (Argille scagliose)*

PLi = *Pliocene inferiore (Argille)*

Ms = *Miocene superiore (Gessi e marne)*

M = *Miocene medio-inferiore*

O-E = *Oligocene-Eocene (calcari-marne)*

Cr = *Cretacico (Calcari)*

G = *Giurassico (Calcari)*

Tr = *Triassico (calcari dolomitici e dolomie)*

Circolazione delle acque.

AGIP Spa

GEDA/GEDI

Allegato 13

Agip

CAMPO DI BOMBA – CURVE DI ISOSUBSIDENZA (in metri) RELATIVE ALLA PRESSIONE DI ABBANDONO

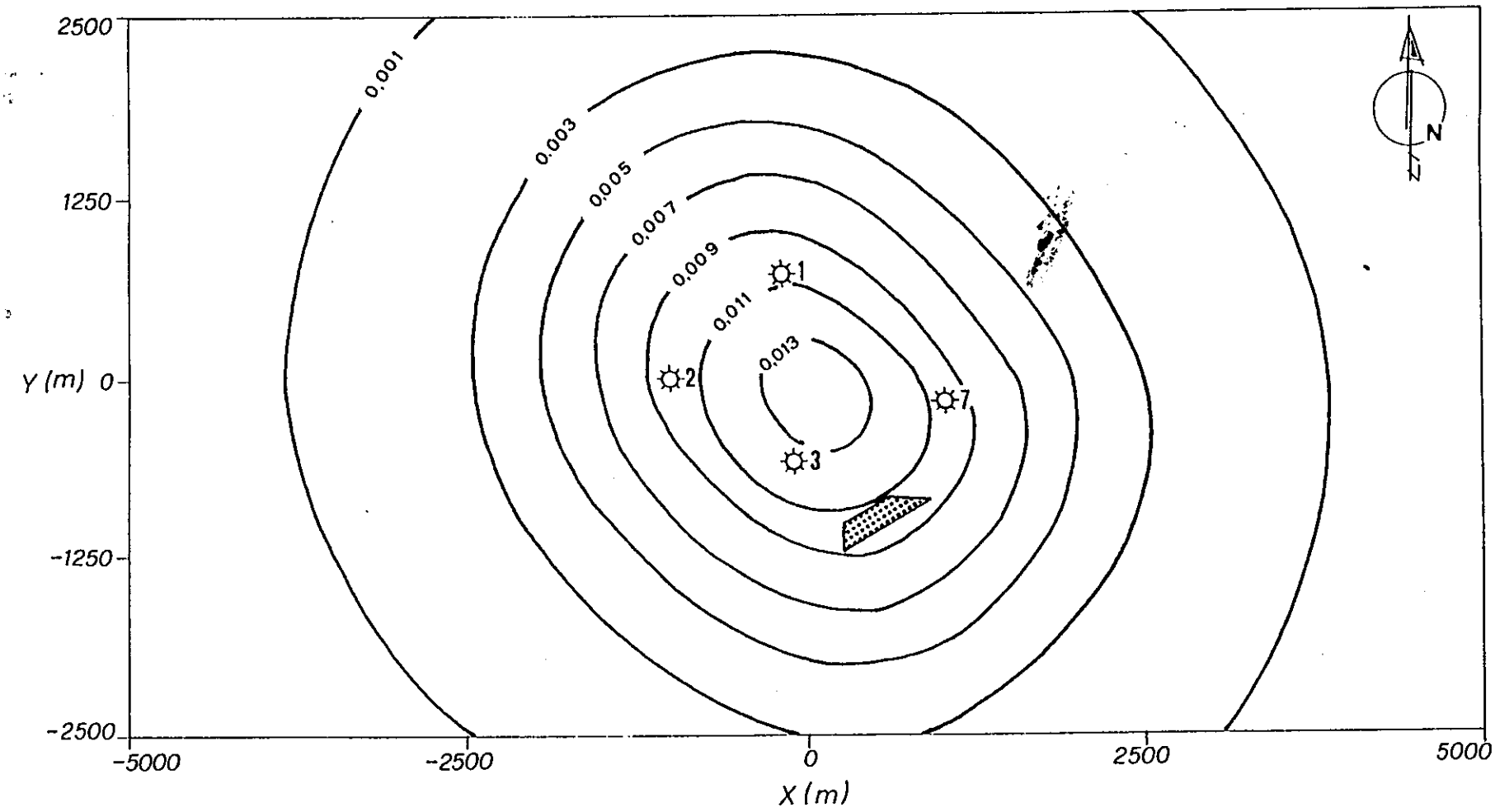

AGIP SPa

GEDA/GEDI

Allegato 14

AGIP Spa GEDA/GEDI

F F BOMBA

435 7 12 8 12 1

13 25 37 48 59 69 COEFFCOMP=.00001344

70 82 94 106 119 132 NU=.25 DP=30

145 156 166 175 184 192

200 212 224 235 246 256

265 273 279 292 305 318

332 346 360 374 388 402

415 427 435

.25 .00001344 30. 62.5

41 21-5000. 2500. 250.

127.0	1180.0	122.0	1200.0	102.0	1250.0	92.0	1280.0
85.0	1310.0	80.0	1326.0	75.0	1345.0	72.0	1345.0
67.0	1360.0	62.0	1380.0	50.0	1400.0	32.0	1440.0
4.0	1500.0	120.0	1180.0	112.0	1220.0	92.0	1260.0
75.0	1300.0	70.0	1340.0	65.0	1370.0	60.0	1390.0
52.0	1400.0	48.0	1400.0	42.0	1405.0	30.0	1427.0
12.0	1458.0	117.0	1195.0	100.0	1240.0	80.0	1280.0
65.0	1310.0	55.0	1350.0	50.0	1390.0	42.0	1410.0
38.0	1425.0	32.0	1430.0	22.0	1440.0	15.0	1460.0
2.0	1490.0	102.0	1220.0	72.0	1260.0	62.0	1290.0
50.0	1315.0	42.0	1340.0	35.0	1380.0	25.0	1410.0
23.0	1437.0	25.0	1414.0	15.0	1467.0	3.0	1480.0
62.0	1250.0	52.0	1280.0	42.0	1300.0	22.0	1330.0
15.0	1360.0	12.0	1380.0	10.0	1405.0	8.0	1434.0
12.0	1460.0	15.0	1480.0	6.0	1495.0	32.0	1280.0
22.0	1310.0	8.0	1330.0	3.0	1360.0	0.0	0.0
0.0	0.0	0.0	0.0	0.0	0.0	0.0	0.0
1.0	1490.0	8.0	1310.0	122.0	1175.0	115.0	1210.0
110.0	1230.0	104.0	1255.0	102.0	1280.0	100.0	1307.0
92.0	1320.0	88.0	1342.0	82.0	1372.0	78.0	1403.0
76.0	1440.0	62.0	1470.0	120.0	1175.0	105.0	1210.0
95.0	1235.0	91.0	1260.0	91.0	1290.0	89.0	1310.0
87.0	1325.0	85.0	1345.0	82.0	1365.0	78.0	1395.0
75.0	1420.0	62.0	1360.0	120.0	1180.0	112.0	1215.0
97.0	1235.0	88.0	1265.0	86.0	1290.0	86.0	1308.0
85.0	1325.0	83.0	1345.0	81.0	1365.0	79.0	1390.0
75.0	1415.0	52.0	1460.0	107.0	1190.0	102.0	1200.0
92.0	1225.0	86.0	1255.0	81.0	1275.0	81.0	1296.0
81.0	1323.0	79.0	1348.0	78.0	1368.0	77.0	1390.0
72.0	1420.0	41.0	1475.0	20.0	1500.0	72.0	1215.0
77.0	1198.0	80.0	1215.0	80.0	1240.0	79.0	1270.0
78.0	1290.0	76.0	1320.0	76.0	1350.0	75.0	1370.0
72.0	1395.0	62.0	1435.0	32.0	1500.0	15.0	1510.0
47.0	1250.0	62.0	1220.0	72.0	1215.0	76.0	1235.0
77.0	1260.0	77.0	1290.0	70.0	1320.0	73.0	1350.0
70.0	1380.0	50.0	1410.0	32.0	1470.0	12.0	1505.0
6.0	1510.0	22.0	1280.0	42.0	1250.0	52.0	1230.0
65.0	1235.0	70.0	1260.0	74.0	1290.0	72.0	1320.0
60.0	1355.0	47.0	1385.0	22.0	1420.0	2.0	1500.0
3.0	1310.0	17.0	1280.0	32.0	1255.0	42.0	1245.0
57.0	1265.0	65.0	1285.0	62.0	1315.0	50.0	1350.0
22.0	1398.0	6.0	1450.0	0.0	0.0	5.0	1310.0
12.0	1280.0	32.0	1260.0	45.0	1265.0	50.0	1280.0

Allegato 15

AGIP Spa GEDA/GEDI

50.0	1310.0	40.0	1355.0	12.0	1500.0	0.0	0.0
0.0	0.0	4.0	1310.0	12.0	1290.0	27.0	1275.0
37.0	1280.0	37.0	1300.0	32.0	1355.0	3.0	1500.0
0.0	0.0	0.0	0.0	0.0	0.0	3.0	1312.0
14.0	1300.0	22.0	1290.0	32.0	1300.0	18.0	1360.0
0.0	0.0	0.0	0.0	0.0	0.0	0.0	0.0
4.0	1320.0	6.0	1315.0	6.0	1320.0	2.0	1360.0
135.0	1180.0	125.0	1210.0	115.0	1230.0	113.0	1245.0
110.0	1270.0	112.0	1295.0	92.0	1320.0	86.0	1345.0
80.0	1380.0	76.0	1410.0	72.0	1450.0	30.0	1480.0
145.0	1175.0	137.0	1208.0	130.0	1230.0	125.0	1250.0
118.0	1280.0	115.0	1300.0	87.0	1330.0	70.0	1360.0
62.0	1390.0	52.0	1425.0	42.0	1460.0	20.0	1480.0
160.0	1180.0	153.0	1210.0	132.0	1240.0	125.0	1280.0
112.0	1305.0	92.0	1320.0	72.0	1360.0	52.0	1390.0
42.0	1415.0	32.0	1440.0	20.0	1480.0	152.0	1200.0
142.0	1220.0	122.0	1250.0	117.0	1300.0	92.0	1320.0
67.0	1340.0	45.0	1380.0	30.0	1410.0	30.0	1430.0
25.0	1460.0	12.0	1480.0	122.0	1220.0	92.0	1235.0
62.0	1265.0	62.0	1300.0	60.0	1338.0	50.0	1360.0
35.0	1385.0	20.0	1415.0	15.0	1440.0	8.0	1475.0
72.0	1260.0	52.0	1265.0	27.0	1280.0	32.0	1330.0
30.0	1360.0	27.0	1375.0	25.0	1395.0	20.0	1420.0
5.0	1440.0	37.0	1310.0	22.0	1320.0	12.0	1350.0
10.0	1400.0	10.0	1405.0	12.0	1402.0	15.0	1405.0
4.0	1440.0	4.0	1380.0	3.0	1400.0	0.0	0.0
0.0	0.0	0.0	0.0	2.0	1430.0	135.0	1165.0
132.0	1198.0	122.0	1230.0	110.0	1260.0	100.0	1280.0
95.0	1295.0	90.0	1300.0	92.0	1320.0	85.0	1240.0
77.0	1265.0	72.0	1390.0	47.0	1420.0	10.0	1490.0
150.0	1160.0	145.0	1185.0	132.0	1215.0	125.0	1240.0
115.0	1250.0	107.0	1265.0	105.0	1280.0	105.0	1305.0
102.0	1340.0	92.0	1360.0	82.0	1390.0	52.0	1440.0
12.0	1495.0	165.0	1155.0	162.0	1170.0	145.0	1200.0
137.0	1220.0	130.0	1238.0	122.0	1270.0	122.0	1280.0
118.0	1310.0	112.0	1340.0	100.0	1360.0	80.0	1395.0
42.0	1440.0	4.0	1490.0	162.0	1175.0	160.0	1158.0
152.0	1175.0	142.0	1200.0	132.0	1220.0	122.0	1250.0
122.0	1280.0	125.0	1315.0	105.0	1340.0	92.0	1365.0
62.0	1495.0	32.0	1440.0	12.0	1490.0	1.0	1510.0
132.0	1195.0	140.0	1185.0	142.0	1180.0	130.0	1190.0
122.0	1210.0	110.0	1250.0	105.0	1285.0	102.0	1320.0
92.0	1345.0	77.0	1370.0	55.0	1395.0	32.0	1440.0
17.0	1490.0	3.0	1510.0	92.0	1240.0	102.0	1230.0
105.0	1210.0	102.0	1205.0	92.0	1220.0	92.0	1260.0
95.0	1290.0	90.0	1320.0	80.0	1350.0	67.0	1375.0
52.0	1400.0	32.0	1455.0	20.0	1490.0	5.0	1510.0
52.0	1300.0	70.0	1300.0	77.0	1265.0	82.0	1240.0
77.0	1245.0	80.0	1270.0	82.0	1300.0	82.0	1330.0
72.0	1355.0	62.0	1380.0	50.0	1400.0	32.0	1460.0
20.0	1500.0	8.0	1510.0	22.0	1360.0	42.0	1340.0
52.0	1300.0	62.0	1280.0	62.0	1270.0	65.0	1285.0
67.0	1310.0	67.0	1340.0	62.0	1360.0	52.0	1385.0

42.0	1410.0	32.0	1465.0	20.0	1500.0	5.0	1510.0
1.0	1410.0	12.0	1400.0	22.0	1360.0	37.0	1320.0
42.0	1290.0	50.0	1300.0	50.0	1320.0	50.0	1345.0
45.0	1370.0	40.0	1390.0	32.0	1430.0	22.0	1480.0
12.0	1505.0	3.0	1510.0	0.0	0.0	0.0	0.0
7.0	1400.0	20.0	1360.0	27.0	1330.0	30.0	1320.0
32.0	1340.0	30.0	1360.0	22.0	1380.0	17.0	1400.0
45.0	1460.0	12.0	1500.0	4.0	1505.0	0.0	0.0
0.0	0.0	0.0	0.0	4.0	1390.0	12.0	1360.0
12.0	1345.0	12.0	1355.0	10.0	1375.0	8.0	1395.0
4.0	1430.0	4.0	1480.0	1.0	1505.0	0.0	0.0
0.0	0.0	0.0	0.0	0.0	0.0	0.0	0.0
2.0	1380.0	2.0	1380.0	2.0	1390.0	0.0	0.0

GIACIMENTO DI BOMBA

PREVISIONE DI COMPORTAMENTO

Caso 1 - Produzione costante di 200.000 [Nm3/g] da 4 pozzi
(pari a 72 * 10E6 [Nm3/anno]) in un arco di trent'anni.

Caso 2 - Produzione costante di 400.000 [Nm3/g] da 4 pozzi
(pari a 144 * 10E6 [Nm3/anno]) in un arco di 15 anni .

GIACIMENTO DI BOMBA - PREVISIONE DI COMPORTAMENTO

(DA RAPPORTI GIAC 16.11.1977 - 20.2.1978)

C A S O 1

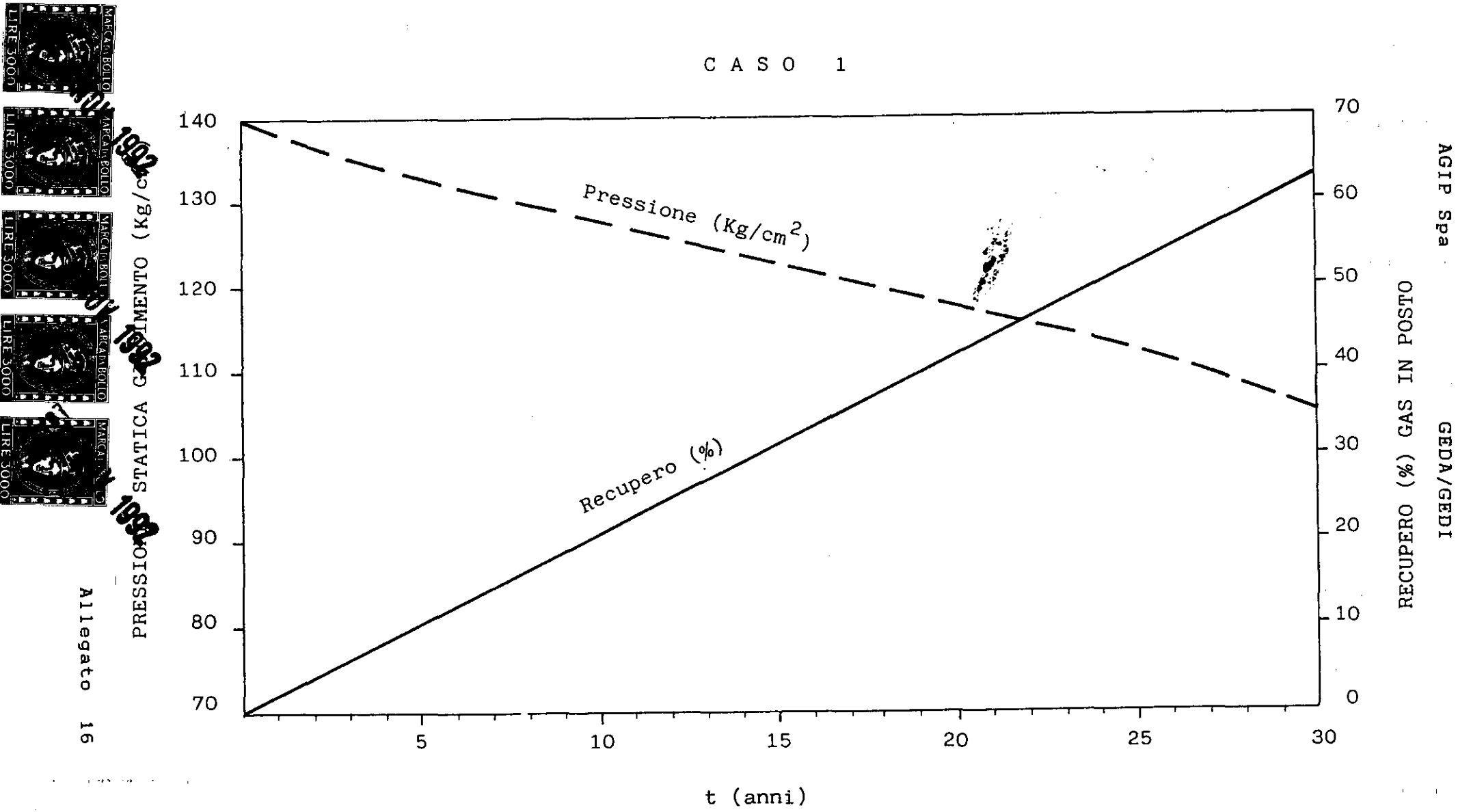

AGIP Spa

GEDA/GEDI

Allegato 16

1992

1993

1994

GIACIMENTO DI BOMBA - PREVISIONE DI COMPORTAMENTO

(DA RAPPORTI GIAC 16.11.1977 - 20.2.1978)

C A S O 2

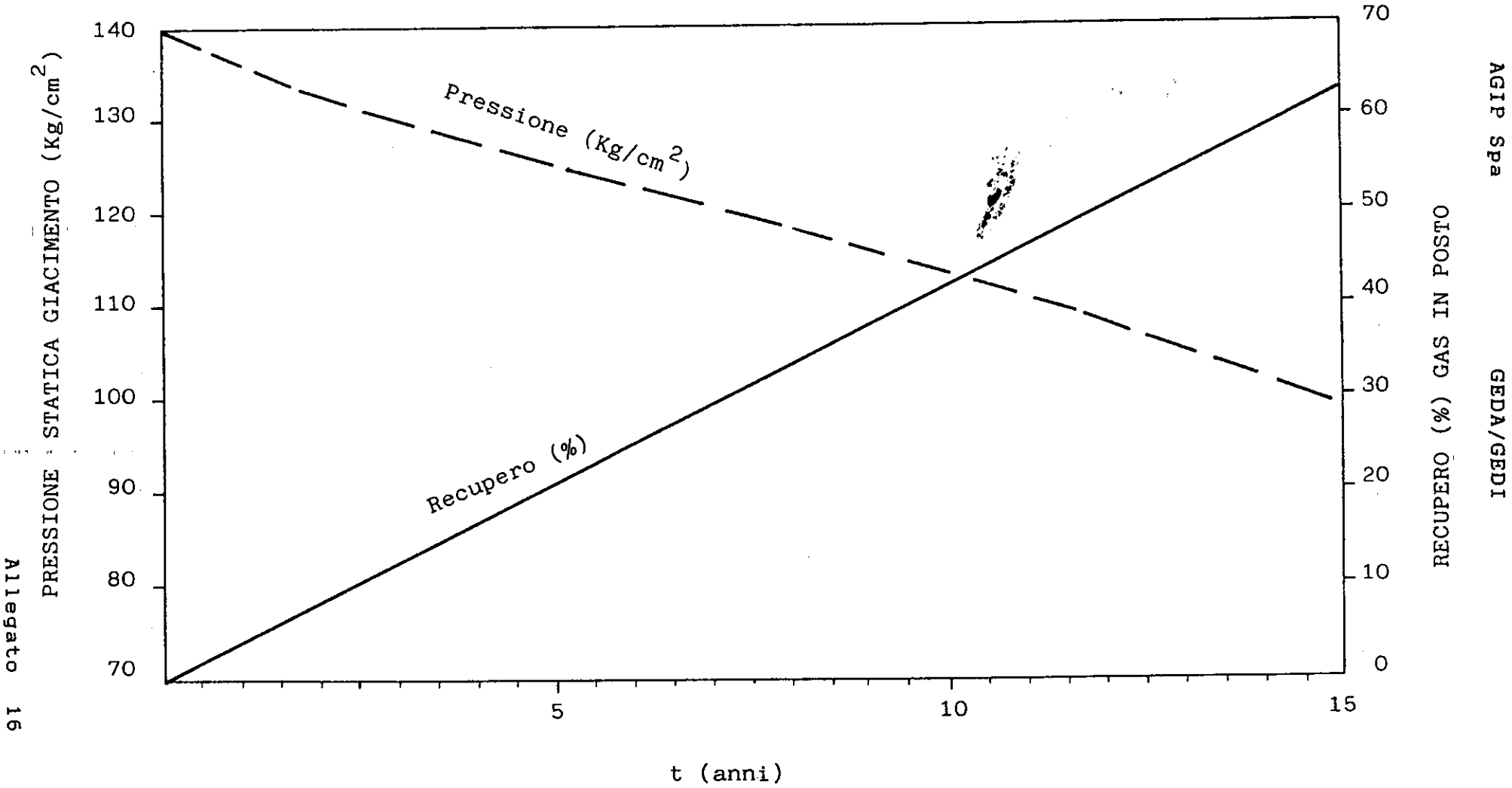

AGIP SpA

GEDA/GEDI

Allegato 16

Land Subsidence Above Compacting Oil and Gas Reservoirs

J. Geertsma, SPE-AIME, Koninklijke/Shell Exploratie en Produktie Laboratorium

Introduction

During the last 20 years, the Royal Dutch/Shell Group has conducted extensive investigations into the phenomenon of reservoir compaction and subsidence. These have included research projects to study subsidence above Bolivar Coast oil reservoirs in Venezuela and to examine the huge Groningen gas reservoir in The Netherlands.

The latter investigation was conducted by a team of specialists from both the Koninklijke/Shell Exploratie en Produktie Laboratorium (KSEPL) and BV Nederlandse Aardolie Maatschappij (NAM), the latter being the producing company owned jointly by Shell and Esso. Details of the Groningen investigation are published elsewhere[24-28] but as it may have consequences for other operating companies working in lowland and other subsidence-prone areas, we shall consider here the causes of subsidence above hydrocarbon-producing reservoirs in a more general way, and review the state of the art of its prediction. A simple method will be presented for estimating the order of magnitude of both compaction and the accompanying subsidence. Application of this method, which can be used to explore the need for an investigation in depth, requires hardly any specialist knowledge. The objective is twofold: to demonstrate that land subsidence due to hydrocarbon production seldom leads to serious subsidence, and to pinpoint the few potential problem areas.

Earlier Field Observations

The literature on subsidence deals mainly with a few notable examples, such as the Goose Creek oil and gas field in Harris County, Tex., where dramatic subsidence occurred between 1918 and 1925,[1,2] and the Wilmington field below Long Beach, Calif.,[3-5] where almost 10 m of subsidence was experienced in 1960. Further subsidence could be avoided in this latter case after unitization and pressure maintenance as a result of water injection. More recently, a search for additional, documented surface depressions over oil and gas fields in the U. S. was reported by Yerkes and Castle.[6] This search revealed only a few other significant cases, mainly fields close to Wilmington, such as those at Buena Vista, Huntington Beach, and Inglewood. From this concentration of subsidence bowls, it may be inferred that such events are somehow related to a similarity in reservoir conditions.

Shell has been confronted only once with a major land-subsidence problem. It is related to the production of oil and gas in Venezuela, where subsidence above a number of important oil reservoirs bordering Lake Maracaibo is a constant phenomenon, and huge dykes have been built to protect the coastal area from flooding. Its cause is discussed by Van der Knaap and Van der Vlis.[7] Subsidence data for oil and gas fields outside the Americas are very scarce indeed. Okumara[8] and Hirono[9] describe a case from the Niigata district of Japan that results from the production of methane dissolved in water. In Italy, AGIP has been accused of contributing to subsidence in the Po Delta by producing from a number of gas fields. However, this area is also plagued by a number

Notable subsidence above producing oil and gas fields is the exception rather than the rule. A simple procedure is outlined to single out the exceptional but real problem areas. This exercise in potential-problem analysis shows that the huge Groningen gas field in The Netherlands is a candidate for causing subsidence troubles in a lowland area.

of other subsidence-generating conditions.

From all the field evidence collected so far, after eliminating obvious hunches and speculations, we must conclude that some or all of the following conditions are fulfilled when considerable subsidence is observed above producing hydrocarbon reservoirs:

1. A significant reduction in reservoir pressure takes place during the production period.
2. Production is effected from a large vertical interval.
3. Oil or gas, or both, are contained in loose or weakly cemented rock.
4. The reservoirs have a rather small depth of burial.

The major productive zones of the Wilmington oil field, for instance, cover seven stacked intervals distributed over a vertical section from 500 to 2,000 m below surface. Oil and gas are produced from sands of varying thicknesses and degrees of consolidation, interbedded with layers of shale or siltstone. The adjacent Inglewood oil reservoir produces from Middle to Upper Pliocene sands over a depth range of 300 to 1,000 m. Commercial production from the Goose Creek field originated at depths between 350 and 1,400 m from unconsolidated sands and clays constituting a productive interval more than 300 m thick. The Lake Maracaibo reservoir rocks are post-Eocene loose sands interbedded with clay. The average depth of burial of these reservoirs is 1,000 m.

Van der Knaap and Van der Vlis[7] have consequently already concluded that subsidence is the result of reservoir compaction. Furthermore, only loose or weakly consolidated rocks seem to be candidates for considerable compaction.

However, we must be careful first to unravel all the factors contributing to reservoir compaction.

Estimating Reservoir Compaction

Reservoir compaction or a reduction in reservoir volume is primarily the result of a reduction in reservoir height. Provided their lateral dimensions are large compared with their height, reservoirs deform predominantly in the vertical plane.[10] *Formation compaction* can therefore be conveniently characterized by the vertical strain in the reservoir, $\varepsilon_z = dz/z$, during production, which expresses the change in height (relative to the initial height) caused by an increase in effective stress due to a reduction in reservoir or pore pressure, p, under constant overburden. *A uniaxial compaction coefficient*, c_m, can then be defined as the formation compaction per unit change in pore-pressure reduction:

$$c_m = \frac{1}{z}\frac{dz}{dp}, \text{ or } \quad \varepsilon_z = c_m dp \quad . \quad . \quad . \quad . \quad (1)$$

(The relationship between c_m and other, better known deformation properties, such as rock bulk compressibility and Poisson's ratio, will be discussed later.) The total reduction in reservoir height can then be expressed as:

$$\Delta H = \int_0^H \int_{p_i}^{p_f} c_m(p, z)\, dp\, dz \quad . \quad . \quad . \quad . \quad . \quad (2)$$

Owing to the very nature of the structure of reservoir rocks, c_m is usually not a constant but a function of effective stress, and thus also of $\Delta p = p_f - p_i$, the difference between future and initial reservoir pressure. However, in many instances it is quite possible to assign a fixed value to the compaction coefficient for the pressure range prevailing during production. Under these circumstances, Eq. 2 simplifies to

$$\Delta H = \int_0^H c_m(z)\, \Delta p(z)\, dz \quad . \quad . \quad . \quad . \quad . \quad (3)$$

This formulation enables us to recognize three individual influences on reservoir-compaction behavior: (1) the reduction in reservoir pressure, (2) the vertical extent of the zone in which pore-pressure reduction takes place, and (3) the order of magnitude of the relevant deformation property of the reservoir rock. Three of the contributions presumed characteristic for subsidence in the previous section are therefore also apparent in this general formulation of formation-compaction behavior.

These elementary considerations show immediately that the combination of a large productive interval, or stack of smaller productive intervals, and a large drop in reservoir-fluid pressure in unconsolidated formations may lead to large compactions. On the other hand, a sizable degree of compaction can be expected even in hard rock for the particular conditions of large pore-pressure reductions and a sufficiently large producing interval.

It is well known that the reduction in reservoir pressure as a function of place and time depends on many factors, such as the mobility, solubility, density, and compressibility of the various pore fluids, as well as on the reservoir boundary conditions (faults, edge or bottom water, etc.). Gas reservoirs show a simpler behavior than most oil reservoirs. In many cases the drop in reservoir pressure from the start of the production period until abandonment is very small. In other instances, particularly in gas and oil reservoirs that produce mainly under the influence of a solution-gas drive, the pore pressure reduction may be considerable.[11] In a gas reservoir, the rate and degree of pore-pressure reduction depend on the permeability distribution, the location of the production wells, and the production rate in relation to the rate of encroaching edge or bottom water. Reservoir simulators are of great help nowadays for predicting pressure distributions as a result of alternative production policies.

In the Groningen gas field, edge water penetrates into the reservoir, mainly from the north, far too slowly to maintain the original reservoir pressure. By about the year 2000, large parts of the reservoir will have experienced a pore-pressure reduction of some 300 kg/cm². The producing interval is large, varying from 90 m in the south, where the production wells are presently concentrated in clusters, to more than 200 m in the north. These figures were sufficiently large to warrant an investigation of the possibility of compaction, the crucial parameter being the compaction coefficient.

The compaction coefficient depends on a number of factors, such as rock type, degree of cementation,

porosity, and depth of burial. From a mechanical point of view, it is the number of contact areas between the individual rock particles and in particular the size and shape of these contacts, that controls rock deformation in sandstones. Similarly in limestones, the shape and strength of the rock skeleton determine rock deformability. Porosity is one of the factors that is frequently influenced by these mechanical contact conditions, but it is certainly not the only one. Effective stress also influences the deformability of the rock skeleton, which accounts for the nonlinear relationship between stress and strain.

The lowest compressibility for sandstone formations is 0.16×10^{-3} cm²/kg, the compaction coefficient of pure quartz. The lower limit for limestones corresponds to the value for calcite; i.e., 0.08×10^{-3} cm²/kg. For sandstones, a rough classification can be made in terms of the degree of cementation: hard, well consolidated, friable or semiconsolidated, and loose sand. As the degree of cementation decreases, there is a gradual transition in the deformation behavior from elastic to cataclastic. Elastic behavior is

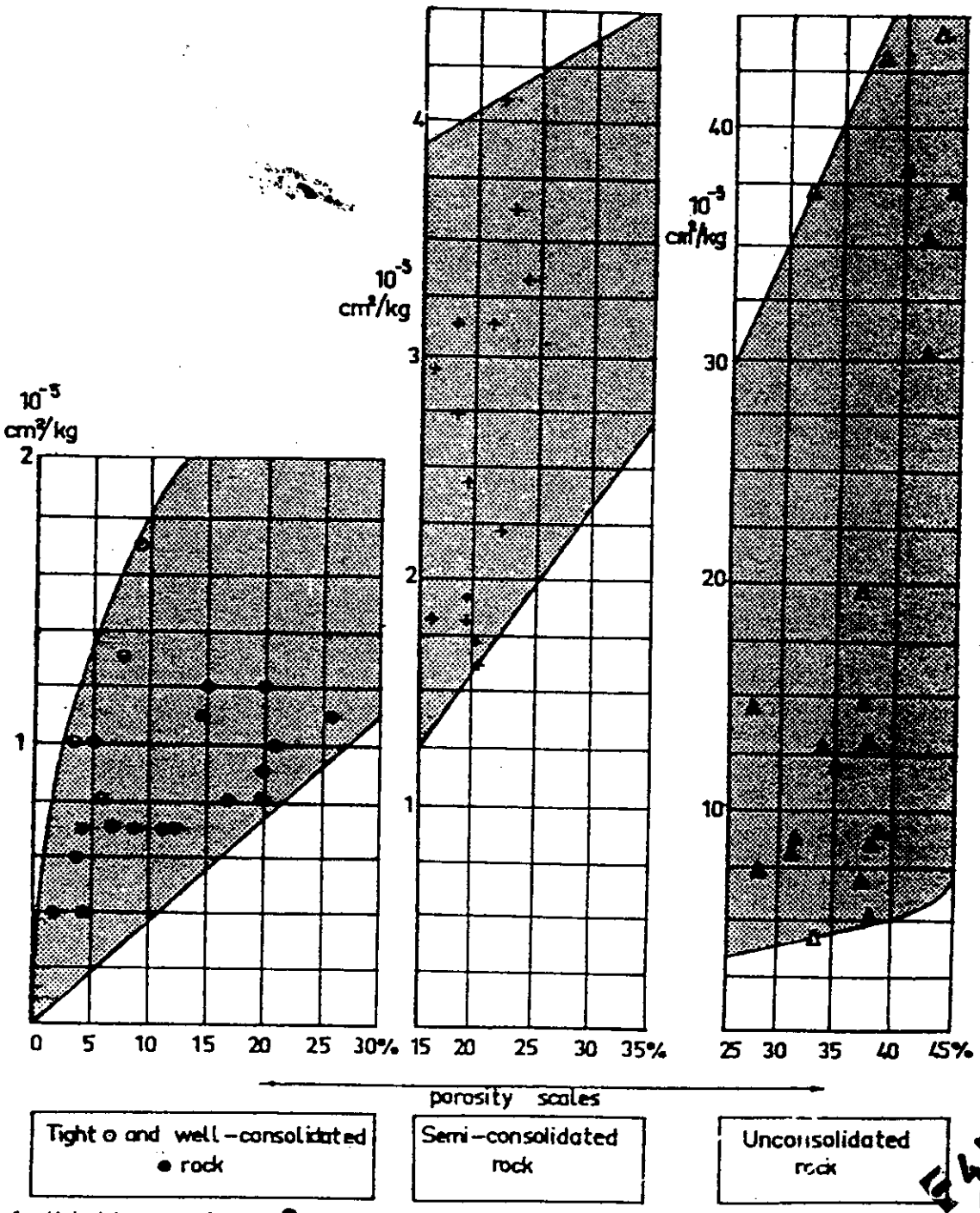

Fig. 1—Uniaxial compaction coefficient, c_m, (vertical axes) for sandstone reservoirs. Effective vertical stress range σ_v = 100 to 200 kg/cm², corresponding to depth of burial of 1,000 m for normally pressured reservoirs.

basically a reversible process, which implies a complete "rebound" during unloading. Catalastic deformation, on the other hand, involves crushing of the particles or other constituents of the framework and is therefore an irreversible process; damage occurs at a number of critically loaded locations, and a permanently denser packing is thus obtained. In practice, it is difficult to determine the elastic:cataclastic deformation ratio uniquely; if one could, it would be attractive to examine a correlation of this ratio with the uniaxial compaction coefficient.

A readily measurable rock property is porosity. High porosity values, up to 40 or 45 percent, apply for loose sands. Hard sandstone formations usually have a low porosity. Even within the above-mentioned categories of degree of cementation, porosity plays a certain role in delineating the compaction coefficient.

Figs. 1 and 2 are an attempt to summarize our large amount of experimental data collected so far for sandstones; they apply to two different preloading[1,2] conditions of interest (corresponding, respectively, to burial depths of approximately 1,000 and

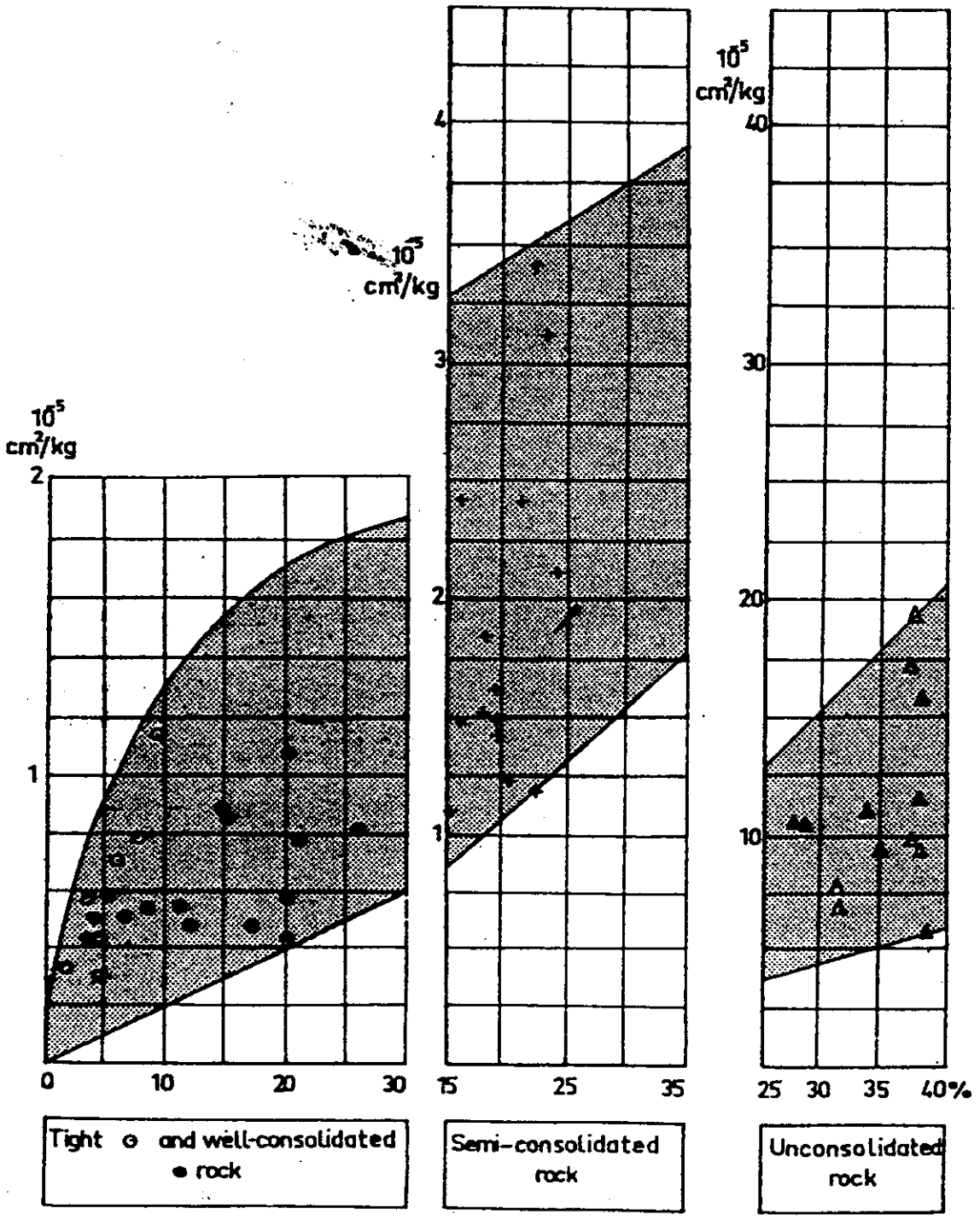

Fig. 2—Uniaxial compaction coefficient, c_m, (vertical axes) for sandstone reservoirs. Effective vertical stress range σ_v = 300 to 600 kg/cm², corresponding to depth of burial of 3,000 m for normally pressurized reservoirs.

3,000 m). Figs. 3 and 4 provide a similar summary of data obtained for limestone reservoirs. Additional figures can be derived from a series of pore-volume compressibility data for both sandstones and limestones published by Newman.[29] A few additional data for unconsolidated sands have been reported by Sawabini *et al.*[30] (For the appropriate conversion formulas, see the section on Procedure for a Detailed Investigation.)

The use of such data can be illustrated by taking the Rotliegend sandstone deposit in which the Groningen gas was found as an example. The material in the Rotliegend reservoir may be described as semi-consolidated. Its depth of burial is about 3,000 m, and the reservoir rock is subjected in situ to an effective prestress of approximately 300 kg/cm². From Fig. 2 it may be concluded that the compaction coefficient must be rather low; somewhere between 1 and 3 × 10^{-5} cm²/kg. This is approximately the compressibility of a good concrete. A small reservoir in this type of rock could hardly show any compaction. However, a combination of the three factors contributing to compaction — i.e., pressure reduction, height of productive interval, and compaction coefficient — produce a compaction figure ranging from 50 to 150 cm; a figure that cannot be overlooked. It is clear that in this case fear of sizable compaction, and thus subsidence, could be experi-

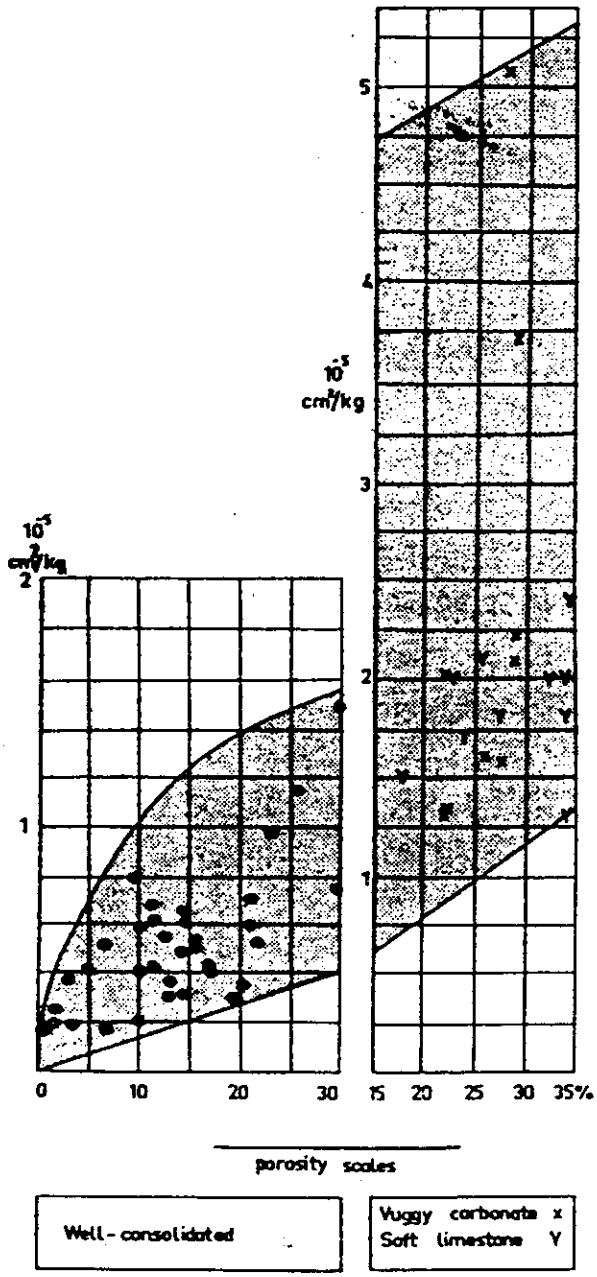

Fig. 3—Uniaxial compaction coefficient, c_m, (vertical axes) for carbonate rock. Effective vertical stress range σ_z = 100 to 200 kg/cm², corresponding to depth of burial of 1,000 m for normally pressured reservoirs.

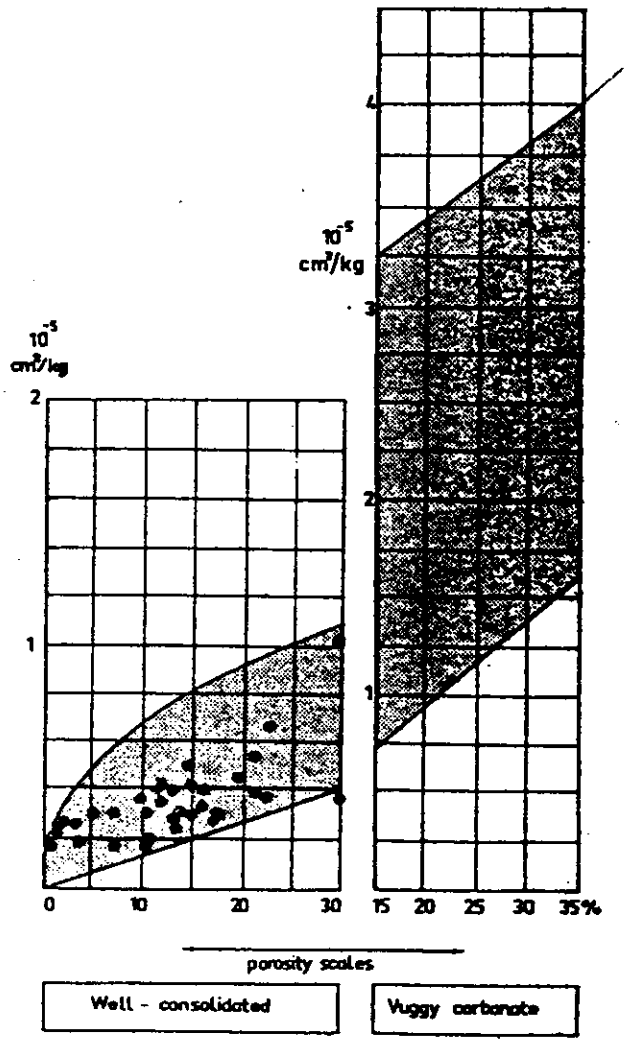

Fig. 4—Uniaxial compaction coefficient, c_m, (vertical axes) for carbonate rock. Effective vertical stress range σ_z = 300 to 600 kg/cm², corresponding to depth of burial of 3,000 m for normally pressured reservoirs.

enced only after the full reservoir dimensions were known in 1964.

If this simple analysis, which takes little time once the appropriate reservoir data are available, predicts compaction figures lower than, say, 10 cm, there is little reason to pursue the matter further. If, on the other hand, larger values are obtained, the compaction/subsidence relationship must also be clarified to establish any consequences in terms of subsidence.

The Subsidence/Compaction Relationship

A first attempt to arrive at a mathematical analysis of subsidence caused by oil-reservoir depletion is due to McCann and Wilts.[12] The objective of their study was a better understanding of the subsidence behavior above the Wilmington field. They investigated the consequences of two different models, both based on elastic continuum mechanics, labeled the "tension center" and the "vertical pincer" model (see Figs. 5A and 5B). Although they concluded that the "tension center" model showed features closely resembling field behavior, whereas the "vertical pincer" model did not, these authors did not subsequently proceed in the proper direction. Consequently, they did not arrive at an explanation for the cause of this similarity to natural behavior, but instead made predictions for future subsidence on the basis of unrealistic combinations of "tension centers".

The problem must be treated mechanically as one of an isolated volume of reduced pore pressure in a porous or nonporous, but elastically deforming, half-space with a traction-free surface. The displacement field in this continuum, and thus also that of its free surface, results from the shrinkage or compaction of the inclusion; if the pore pressure decreases, the effective stress on the rock skeleton increases correspondingly throughout the inclusion. We wish to determine the interaction between the shrinking inclusion and its surroundings to which it is connected. This interaction can be calculated with the help of the theory of poroelasticity, sometimes inappropriately called the "theory of consolidation". This theory is mathematically similar to that of thermoelasticity. A number of authors[13-15] have discussed and applied this similarity in the past. The present poroelastic problem can be analyzed most conveniently with the help of the so-called nucleus-of-strain concept in the half-space, as introduced by Mindlin and Cheng[16] and, independently, by Sen[17] in the theory of thermoelasticity. From this concept and its results, it follows that the subsidence — i.e., the displacement perpendicular to the free surface due to a nucleus of strain of small but finite volume, V — under the influence of a pore-pressure reduction, Δp, amounts to

$$u_z(r,0) = -\frac{1}{\pi} c_m(1-\nu) \frac{D}{(r^2+D^2)^{3/2}} \Delta pV. \quad \ldots\ldots\ldots\ldots\ldots\ldots (4)$$

For the elastic deformation constants that can be introduced into this relationship, we again selected the uniaxial compaction coefficient, c_m, in addition to Poisson's ratio, ν. The depth of burial of the nucleus of strain is indicated by D, and r is the radial distance from the vertical axis through the nucleus.

Similarly, the horizontal surface movement, which may be of interest if serious surface deformations are to be expected, amounts to

$$u_r(r,0) = +\frac{1}{\pi} c_m(1-\nu) \frac{r}{(r^2+D^2)^{3/2}} \Delta pV. \quad \ldots\ldots\ldots\ldots\ldots\ldots (5)$$

Apart from the proportionality constant, which in the present formulation acquires a clear physical meaning, these expressions are similar to those found by McCann and Wilts for their "tension center" model. It also follows that the ratio of the horizontal and vertical surface displacements above such a nucleus of strain amounts to $-r/D$.

The results of the nucleus-of-strain concept can be applied to real reservoir conditions in a number of ways. Much information can be obtained from an analysis of the deformation pattern around a disc-shaped reservoir of thickness H and radius R at depth

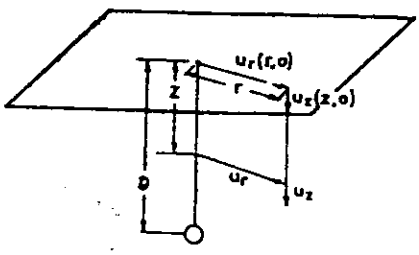

$$u_z(r,o) = \frac{2(1-\nu)C}{G} \frac{D}{(r^2+D^2)^{1/2}}$$

$$u_r(r,o) = \frac{2(1-\nu)C}{G} \frac{r}{(r^2+D^2)^{1/2}}$$

$C = \frac{t_i a^3}{2}$; t_i = TENSION PER UNIT AREA OVER SURFACE OF TENSION SPHERE;

a = RADIUS OF TENSION SPHERE

Fig. 5A—Spherical-tension model of McCann and Wilts.[12]

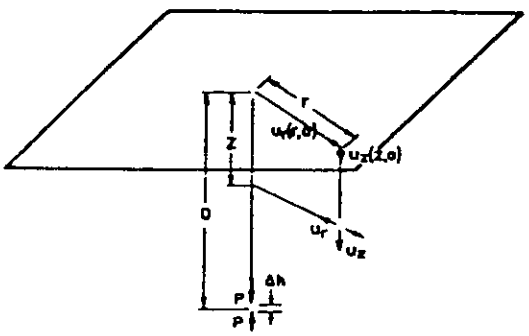

$$u_z(z,o) = \frac{5M}{8\pi G} \frac{D}{(r^2+D^2)^{3/2}} \left\{ \frac{6D^2}{5(r^2+D^2)} - \frac{4\nu}{5} \right\}$$

$$u_r(r,o) = \frac{5M}{8\pi G} \frac{r}{(r^2+D^2)^{3/2}} \left\{ \frac{1}{3(1-\nu)} \left[\left[2-(1-2\nu)^2 \right] - \frac{3D^2(3-2\nu)}{r^2+D^2} \right] \right\}$$

M = PΔh P = STRENGTH OF VERTICAL FORCES
Δh = EFFECTIVE SEPARATION OF FORCES

Fig. 5B—Vertical-pincer model of McCann and Wilts.[12]

D for a uniform reservoir pressure reduction Δp throughout the reservoir. Such an idealized reservoir shape has been suggested before[18] and has been studied in more detail by Evangelisti and Poggi.[19] The latter authors did not include an explanation of how solutions could be obtained in closed form, but instead provided computer data. To perform rather simple calculations, one need only assume that the solution is not too adversely influenced by treating both the reservoir and its surroundings as homogeneous with respect to their deformation properties: both c_m and ν must be assumed to be constant throughout the entire half-space. With the help of this assumption, the subsidence above a disc-shaped reservoir can be found by integrating the nucleus solution over the entire reservoir volume.[25] After the necessary mathematical manipulations, one obtains

$$u_z(r, 0) = -2c_m(1-\nu)\Delta p H R \int_0^\infty e^{-D\alpha} J_1(\alpha R) J_0(\alpha r)\, d\alpha \quad . \quad . \quad (6)$$

and

$$u_r(r, 0) = +2c_m(1-\nu)\Delta p H R \int_0^\infty e^{-D\alpha} J_1(\alpha R) J_1(\alpha r)\, d\alpha, \quad . \quad . \quad (7)$$

in which J_0 and J_1 are Bessel functions of zero and first order, respectively. Numerical values of these "Hankel-Lipschitz integrals" have been reported by Eason *et al.*[20] After introducing the dimensionless ratios $\rho = r/R$ and $\eta = D/R$ and the shorthand notation

$$u_z(r, 0) = -2c_m(1-\nu)\Delta p H A(\rho, \eta),$$

$$u_r(r, 0) = +2c_m(1-\nu)\Delta p H B(\rho, \eta),$$

we can use Table 1 and 2, which list A and B for a selected number of values of ρ and η.

It has been shown in Ref. 8 that the first row in Table 1 can also be determined, where $A = A(0, \eta)$, from the more simple formulation

$$u_z(0, 0) = -2c_m(1-\nu)\Delta p H \left(1 - \frac{\eta}{\sqrt{1+\eta^2}}\right) \quad . \quad . \quad . \quad . \quad . \quad . \quad . \quad . \quad . \quad . \quad . \quad . \quad (6a)$$

Also, since reservoir compaction amounts to $c_m \Delta p H$, we may write

$$\frac{\text{Subsidence}}{\text{Reservoir compaction}} = -2(1-\nu)A,$$

$$\text{which means} \sim -1.5A \quad . \quad . \quad . \quad . \quad (8)$$

$$\frac{\text{Horizontal surface displacement}}{\text{Reservoir compaction}} = 2(1-\nu)B,$$

$$\text{or} \sim 1.5B. \quad . \quad . \quad . \quad . \quad . \quad . \quad . \quad . \quad . \quad . \quad . \quad . \quad (9)$$

Thus the ratio between maximum subsidence and reservoir compaction is in essence determined by the ratio η between depth of burial and the lateral extent of the reservoir. Small, deeply buried reservoirs are

TABLE 1—VALUES OF $A = R \int_0^\infty J_1(\alpha R) J_0(\alpha r)\, e^{-D\alpha}\, d\alpha$ FOR RANGES OF VALUES OF $\rho = r/R$ AND $\eta = D/R$

ρ	η 0.0	0.2	0.4	0.6	0.8	1.0	1.2	1.4	1.6	1.8	2.0	3.0
0.0	1.0000	0.8039	0.6286	0.4855	0.3753	0.2929	0.2318	0.1863	0.1520	0.1258	0.1056	0.0513
0.2	1.0000	0.7983	0.6201	0.4771	0.3683	0.2876	0.2279	0.1835	0.1500	0.1244	0.1045	0.0510
0.4	1.0000	0.7789	0.5924	0.4508	0.3473	0.2720	0.2167	0.1754	0.1442	0.1202	1.1014	0.0502
0.6	1.0000	0.7349	0.5377	0.4043	0.3124	0.2470	0.1989	0.1628	0.1351	0.1135	0.0965	0.0488
0.8	1.0000	0.6301	0.4433	0.3368	0.2658	0.2147	0.1762	0.1465	0.1234	0.1049	0.0901	0.0470
1.0	0.5000	0.3828	0.3105	0.2559	0.2130	0.1787	0.1510	0.1286	0.1102	0.0951	0.0827	0.0449
1.2	0.0000	0.1544	0.1871	0.1795	0.1621	0.1433	0.1257	0.1103	0.0965	0.0848	0.0748	0.0424
1.4	0.0000	0.0717	0.1101	0.1216	0.1197	0.1120	0.1024	0.0925	0.0831	0.0744	0.0667	0.0398
1.6	0.0000	0.0400	0.0682	0.0829	0.0876	0.0865	0.0824	0.0768	0.0707	0.0646	0.0589	0.0370
1.8	0.0000	0.0249	0.0449	0.0580	0.0647	0.0668	0.0659	0.0633	0.0597	0.0557	0.0516	0.0343
2.0	0.0000	0.0168	0.0312	0.0418	0.0485	0.0519	0.0528	0.0520	0.0502	0.0477	0.0450	0.0315
3.0	0.0000	0.0042	0.0082	0.0118	0.0149	0.0174	0.0193	0.0207	0.0216	0.0221	0.0222	0.0198

TABLE 2—VALUES OF $B = R \int_0^\infty J_1(\alpha R) J_1(\alpha r)\, e^{-D\alpha}\, d\alpha$ FOR RANGES OF VALUES OF $\rho = r/R$ AND $\eta = D/R$

ρ	η 0.0	0.2	0.4	0.6	0.8	1.0	1.2	1.4	1.6	1.8	2.0	3.0
0.0	0.0000	0.0000	0.0000	0.0000	0.0000	0.0000	0.0000	0.0000	0.0000	0.0000	0.0000	0.0000
0.2	0.1015	0.0954	0.0804	0.0628	0.0472	0.0350	0.0259	0.0194	0.0147	0.0113	0.0089	0.0032
0.4	0.2134	0.1979	0.1622	0.1238	0.0917	0.0675	0.0500	0.0375	0.0285	0.0220	0.0173	0.0062
0.6	0.3530	0.3163	0.2443	0.1789	0.1298	0.0949	0.0703	0.0529	0.0405	0.0314	0.0248	0.0090
0.8	0.5721	0.4573	0.3151	0.2197	0.1570	0.1147	0.0854	0.0648	0.0500	0.0391	0.0311	0.0117
1.0	∞	0.5456	0.3422	0.2355	0.1693	0.1252	0.0945	0.0726	0.0567	0.0448	0.0359	0.0139
1.2	0.5235	0.4278	0.3072	0.2237	0.1666	0.1265	0.0976	0.0764	0.0605	0.0485	0.0393	0.0158
1.4	0.3293	0.3026	0.2482	0.1958	0.1535	0.1208	0.0958	0.0766	0.0619	0.0504	0.0414	0.0174
1.6	0.2338	0.2228	0.1962	0.1650	0.1358	0.1110	0.0907	0.0743	0.0611	0.0506	0.0422	0.0185
1.8	0.1767	0.1711	0.1566	0.1377	0.1180	0.0997	0.0838	0.0703	0.0590	0.0496	0.0420	0.0194
2.0	0.1390	0.1358	0.1272	0.1152	0.1018	0.0885	0.0762	0.0653	0.0559	0.0478	0.0410	0.0199
3.0	0.0580	0.0576	0.0562	0.0541	0.0514	0.0483	0.0449	0.0414	0.0380	0.0346	0.0314	0.0190

therefore hardly capable of producing significant subsidences, even if their reservoir compaction cannot be neglected. In contrast, extremely large reservoirs at large depths may be potential candidates for subsidence.

In order to illustrate the deformation pattern of compacting reservoirs and their surroundings in more detail, Fig. 6 exaggerates the vertical-displacement distribution at the surface, as well as at the top and bottom of the reservoir. Two practical ratios $\eta = D/R$ are used for this illustration: 1.0 and 0.2. For $\eta = 1.0$, subsidence is about 0.45 times reservoir compaction. For $\eta = 0.2$, subsidence is much larger for the same degree of compaction; i.e., 1.20 times reservoir compaction. It is thus seen that subsidence may exceed compaction for homogeneous rock conditions, the maximum ratio being $2(1 - \nu)$. Figs. 7 and 8 provide details of these deformation patterns.

To date no field cases have been reported of subsidence above reservoirs at depths exceeding 2,000 m. However, the theory certainly does not exclude this possibility. In practice, the chances of severe subsidence above deeply buried oil or gas reservoirs are small for the following reasons:

1. The value of uniaxial-compaction coefficient decreases with increasing effective stress (see Figs. 1 through 4). Because reservoirs frequently experience a hydrostatic pore pressure before production, the original effective stress will increase with depth of burial of the reservoir, and the degree of compaction will therefore be reduced.

2. To provide similar η-values, deep reservoirs must have a larger lateral extent than shallow ones.

On the other hand, deep reservoirs can be subjected to a larger ultimate reduction in reservoir pressure compared with what is physically possible in shallow reservoirs. This means, for instance, that giant gas reservoirs are in principle candidates for subsidence, even if they are situated at great depth. We have come to the conclusion that the Groningen gas field, for which $\eta < 0.20$ and for which ultimate compaction may reach a value of 1 m, is such a case.

Procedure for a Detailed Investigation

A survey of the likelihood of both compaction and subsidence in the way indicated above reveals that there are only a few candidates for further analysis, if we take 10 cm as an acceptable but already difficult to analyze subsidence measure. According to core analyses, NAM's Schoonebeek oil reservoir must show a small subsidence of this order of magnitude. Careful levelling surveys indeed show small surface movements, but the displacement rate is too small to allow a detailed comparison between theory and practice.

It is not even justified to take a fixed order of magnitude as a universal tolerance limit; the latter depends both on the location of the reservoir in relation to residential or industrial areas, and on the acceptability of flooding or other surface calamities. The compaction of offshore reservoirs, or reservoirs beneath the desert or a tropical forest, may have to be analyzed for reservoir-engineering studies, but probably not in the light of local subsidence, unless, for example, a large dam is or will be located in the neighborhood, or an active fault plane may be mobilized.

Nevertheless, our technical survey confirms what has been observed in practice; namely, that detailed and costly investigations are necessary only in a very restricted number of cases. Such an investigation involves a series of steps, which we shall outline in the following section.

Laboratory Measurement of the Uniaxial-Compaction Coefficient on Representative Core Samples

The technical difficulties are related to equipment design, the selection of representative core material, and the interpretation of the measurements.

Equipment Design. The uniaxial compaction of *loose sands and clays* can best be measured with the help of an oedometer-type cell. A great deal of care must be taken when cutting the samples from rubber-sleeve cores and mounting them in the cell with the least possible distortion. The most compressible parts of the core material are frequently the most vulnerable during both recovery and laboratory handling. *Well consolidated and friable rocks* can be studied either in a triaxial cell with zero lateral deformation, or in a hydrostatic loading cell. As has been pointed out by Teeuw,[21] the first method is the more accurate and also allows measurement of Poisson's ratio; however, it is also the more elaborate technique. The second procedure can be carried out rapidly in a rather simple setup and is thus better suited for routine measurements. A formula relates uniaxial and hydrostatic compaction data:

$$c_m = \frac{1}{3}\left(\frac{1+\nu}{1-\nu}\right)(1-\beta)\,c_b, \quad \ldots \quad (10)$$

where

c_b = hydrostatically determined bulk compressibility.

ν = Poisson's ratio, for which an estimated value of 0.25 to 0.30 can be used for most reservoir rocks. ν can also be measured for a selected number of cores in the triaxial cell.

β = ratio between rock matrix and rock bulk compressibility $= c_r/c_b$. This ratio can be determined for sands and sandstones on the basis of the c_r value of quartz, and for

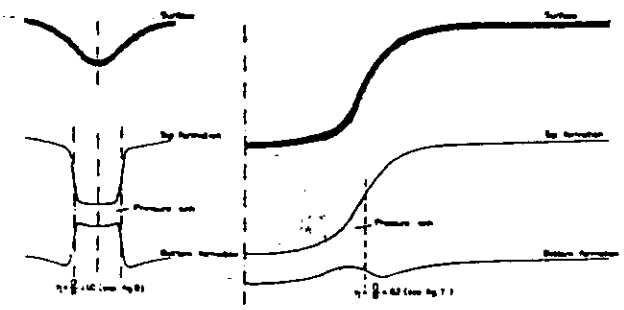

Fig. 6—Compaction and subsidence.

limestones on the basis of the c_r value of calcite. The larger c_b, the smaller β and thus the smaller its influence on c_m.

As a less practical alternative, Eq. 10 can be written in the form

$$c_m = \frac{1}{2G}(1-\beta)\left(\frac{1-2\nu}{1-\nu}\right), \quad \ldots \quad (11)$$

where G represents the shear modulus.

Eq. 10 is also useful to obtain an impression of the appropriate deformation constant for subsidence analysis from rock bulk-compressibility or pore-compressibility data published elsewhere, the latter being $1/\phi$ times the former, if ϕ represents porosity. Note that because as an average

$$\frac{1}{3}\left(\frac{1+\nu}{1-\nu}\right)(1-\beta) = c_m/c_b = 0.5/0.7,$$

c_m is considerably smaller than the bulk compressibility, c_b.

Selection of Representative Core Material. The degree of homogeneity or heterogeneity of the reservoir must be established, which means that logs must be examined and information must be obtained from reservoir geologists to gain a good impression of reservoir conditions. For a recently discovered field, many questions cannot be answered in detail until sufficient wells have been drilled and analyzed.

It must also be realized that both the least compressible and the most compressible rock samples must be tested in proportion to their relative abundance in the reservoir.

Interpretation of Measurements. The measurements provide a curve of displacement or strain as a function of effective stress (above natural level). The original stress level cannot be measured in the field, but must be estimated on the basis of reasonable assumptions. The precise initial loading condition for the laboratory experiment cannot therefore be established with certainty.

A more serious problem, which has yet to be overcome, is unloading of the core material during core recovery in the well; thus an unloading/reloading cycle always precedes a laboratory experiment. As explained previously, part of the rock deformation process is irreversible, so that we are always dealing with a somewhat distorted sample. As a consequence, the laboratory experiments probably provide compressibility figures for the first loading cycle that are too high.

Determination of the Compaction Distribution In the Reservoir

The compaction distribution can be derived by judiciously combining the data obtained using the approach described in the section of Equipment Design with other relevant reservoir data, which include the following:

1. A map showing the vertical and lateral distributions of the productive zone. The words "productive zone" must be considered here in a somewhat different context compared with their interpretation in reservoir engineering. The "productive zone" for compaction analysis includes all zones where the pore pressure will be reduced, irrespective of whether they contain hydrocarbons or not.
2. A prediction of the reservoir-pressure distribution as a function of place and time, presumably based on an appropriate numerical analysis (reservoir simulator).

Both these items gain in accuracy the better the reservoir has been explored. This means that in practice the predictions of compaction and subsidence must be updated periodically when more pertinent information becomes available.

3. Attempts have been made to correlate laboratory compaction data with petrophysical properties measured or derived from logs. Even a vast number of core samples represent a very small fraction of the reservoir rock. Sonic and formation-density logs have been considered for this purpose, but such at-

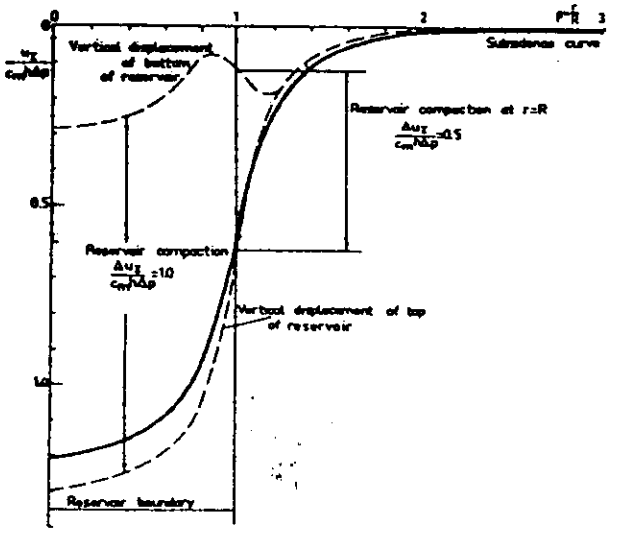

Fig. 7—Compaction and subsidence for $\eta = D/R = 0.2$ and $\nu = 0.25$.

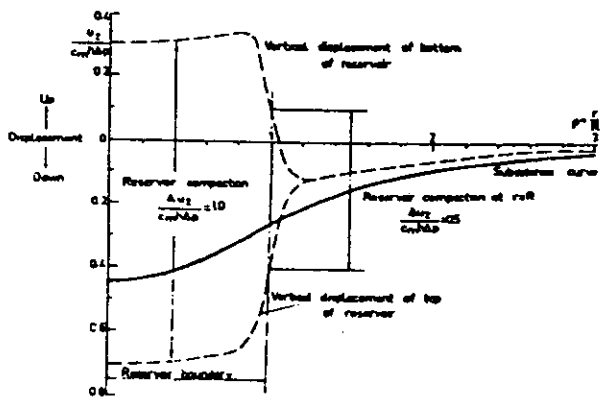

Fig. 8—Compaction and subsidence for $\eta = D/R = 1.0$ and $\nu = 0.25$.

tempts have not been successful.[25] The best correlation established so far is between compaction coefficient and log-derived porosity values, although there is still a wide scatter. The sonic log shows a good correlation with compaction for hard rocks, but these are the least interesting for a study of compaction and subsidence. The cataclastic deformation properties of friable and loose rock material are not reflected in the known petrophysical properties measured in a wellbore.

Determination of the Subsidence Profile

This can be derived from the compaction distribution on the basis of the theory of poroelasticity. Because complex geometries are usually involved, as well as various degrees of heterogeneity both in and outside the reservoir, numerical techniques such as finite-element[22] or finite-difference procedures can be used to calculate the compaction/subsidence relationship. To apply these techniques in three-dimensional space to any advantage, however, one must be able to specify the input data with sufficient detail to justify such a sophisticated approach.

A certain degree of inaccuracy or uncertainty must always be accepted in specifying the spatial distribution of compaction within the reservoir. The value and distribution of the deformation properties of the reservoir surroundings are known with even less accuracy, as there are fewer core and log data available. For more or less homogeneous conditions, we have developed a method that treats reservoirs of arbitrary three-dimensional shape and pressure distribution.[26] The analytical concept of elastic deformations caused by nuclei of strain according to Eqs. 4 and 5 can still be used in this application, but integration over the entire reservoir volume must be replaced by summation of the effect of a finite number of nuclei of strain, which together represent the reservoir volume. An individual pore-pressure reduction can be assigned to each nucleus. The summation is performed by a digital computer.

Important aspects of the subsidence/compaction relationship, such as the ratio between the volume of the subsidence bowl and the reduction in reservoir volume, as well as the subsidence profile, are influenced by contrasts in deformability between reservoir and underlying formations. For the Groningen gas field the deformability of the reservoir is rather small and seems to be of the same order of magnitude as that of the overlying and underlying formations. This means that, according to the theory, the subsidence volume may exceed the reduction in pore volume. Conversely, under Bolivar Coast conditions these volumes are approximately equal, because here the basement rock is very stiff compared with the highly deformable loose sands and clay layers that constitute the reservoirs.

The nuclei-of-strain concept can even be applied to analyze the latter type of conditions, provided the surface deformations $u_z(r,0)$ and $u_r(r,0)$ for a nucleus are tabulated from a finite-element analysis of the heterogeneous half-space. There is a restriction in that the deformation contrasts must be due to horizontal layering. Provided this approximates the real situation, the numerical procedure of summing the effect of a finite number of nuclei of strain is still a valid one for obtaining the subsidence profile above a reservoir of arbitrary lateral shape.

Lastly, in problem areas such research work must be accompanied by in-situ compaction measurements in observation wells and levelling surveys during the production period. The costs of this field work constitute the main expense and it should be carried out only if the severity of the problem justifies it.

Conclusions

Subsidence is the result of reservoir compaction, which in turn depends on the product of reservoir-pressure reduction, height of productive interval, and rock compressibility. The relevant compressibility factor is the uniaxial-compaction coefficient, which varies between 0.3×10^{-6} cm²/kg for tight rock and 20 to 40 $\times 10^{-3}$ cm²/kg for loose sands. The lower the effective stress level the higher the maximum possible compaction coefficient for a loose sand. The amount of subsidence resulting from reservoir compaction depends mainly on the ratio between the depth of burial and the lateral extent of the reservoir. For subsidence to equal compaction, a reservoir at a depth of 1,000 m must have a surface area of not less than 50 km².

In applying these findings to a judgment of the frequency of occurrence of major subsidence above oil and gas fields, it must be remembered that in many oil reservoirs the reduction in reservoir pressure is small throughout the production period. Exceptions are oil reservoirs that produce by means of a dissolved-gas drive. Pressure maintenance may be of advantage from a recovery point of view, and the reservoir engineer will therefore automatically consider injection of water or gas for artificial pressure maintenance. Gas reservoirs can be produced only by expansion; water injection may have an adverse effect on the recovery factor and is therefore usually unattractive.

On the basis of these crude generalizations, it may be concluded that oil reservoirs of the depletion type in loose sands, and extremely large gas reservoirs in either loose or friable rocks, are most sensitive to subsidence. Other reservoirs cannot give rise to real concern in this respect.

Nomenclature

c_b = rock bulk compressibility
c_m = uniaxial compaction coefficient
c_r = rock matrix compressibility
D = depth of burial
G = shear modulus
H = height of productive interval
Δp = pore (reservoir) pressure reduction
r = radius
R = reservoir radius
u_r = radial displacement
u_z = vertical displacement
V = volume of a nucleus of strain
z = vertical coordinate
$\beta = c_r/c_b$
ϵ_z = vertical strain $= dz/z$

$\eta = D/R$
ν = Poisson's ratio
$\rho = r/R$
ϕ = porosity

Acknowledgments

Prof. U. S. Grant kindly provided Ref. 12, and Prof. G. L. Chierici, Ref. 19. I wish to thank in particular D. Teeuw for providing the details on laboratory-compaction measurements, G. van Opstal for stimulating discussions on the subsidence/compaction relationship, and the management of Shell Research NV for permission to publish this paper.

References

1. Pratt, W. E. and Johnson, D. W.: "Local Subsidence of the Goose Creek Field," *J. of Geology* (1926) **34**, 577.
2. Snider, L. C.: "A Suggested Explanation for the Surface Subsidence in the Goose Creek Oil and Gas Field, Texas," *Bull.*, AAPG (1927) **11**, 729.
3. Gilluly, J. and Grant, U. S.: "Subsidence in the Long Beach Harbor Area, California," *Bull.*, GSA (1949) **60**, 461.
4. Mayuga, M. N. and Allen, D. R.: "Subsidence in the Wilmington Oil Field, Long Beach, California, U. S. A.," *Land Subsidence*, Publication No. 88, AIHS-UNESCO (no date of issue) **I**, 66.
5. Allen, D. R.: "Physical Changes of Reservoir Properties Caused by Subsidence and Repressurizing Operations, Wilmington Field, California," *J. Pet. Tech.* (Jan., 1968) 23-29.
6. Yerkes, R. F. and Castle, R. O.: "Surface Deformation Associated with Oil and Gas Field Operations in the United States," *Land Subsidence*, Publication No. 88, AIHS-UNESCO (no date of issue) **I**, 55.
7. Van der Knaap, W. and Van der Vlis, A. C.: "On the Cause of Subsidence in Oil-Producing Areas," *Proc.*, 7th World Pet. Cong., Mexico City (1967) **3**, 85.
8. Okumara, T.: "Analysis of Land Subsidence in Niigata," *Land Subsidence*, Publication No. 88, AIHS-UNESCO (no date of issue) **I**, 130.
9. Hirono, T.: "Niigata Ground Subsidence and Ground Water Change," *Land Subsidence*, Publication No. 88, AIHS-UNESCO (no date of issue) **I**, 144.
10. Geertsma, J.: "The Effect of Fluid Pressure Decline on Volume Changes of Porous Rocks," *Trans.*, AIME (1957) **210**, 331-339.
11. De Haan, H. J. and van Lookeren, J.: "Early Results of the Large-Scale Steam Soak Project in the Tia Juana Field, Western Venezuela," *J. Pet. Tech.* (Jan., 1969) 101-110; *Trans.*, AIME, **246**.
12. McCann, G. D. and Wilts, C. H.: "A Mathematical Analysis of the Subsidence in the Long Beach-San Pedro Area," internal report, California Institute of Technology, Pasadena (Nov., 1951).
13. Lubinski, A.: "The Theory of Elasticity for Porous Bodies Displaying a Strong Pore Structure," *Proc.*, 2nd U. S. Natl. Cong. of Applied Mechanics (1954) 247.
14. Biot, M. A.: "General Solutions of the Equations of Elasticity and Consolidation for a Porous Medium," *J. Applied Mech.* (1956) **23**, 91.
15. Geertsma, J.: "A Remark on the Analogy Between Thermoelasticity and the Elasticity of Saturated Porous Media," *J. Mech. Phys. Solids* (1957) **6**, 13.
16. Mindlin, R. D. and Cheng, D. H.: "Thermo-Elastic Stress in the Semi-Infinite Solid," *J. Applied Phys.* (1950) **21**, 931.
17. Sen, B.: "Note on the Stress Produced by Nuclei of Thermoelastic Strain in a Semi-Infinite Elastic Solid," *Quarterly Applied Math.* (1950) **8**, 635.
18. Geertsma, J.: "Problems of Rock Mechanics in Petroleum Production Engineering," *Proc.*, 1st Cong. of the Intl. Soc. of Rock Mech., Lisbon (1966) **I**, 585.
19. Evangelisti, G. and Poggi, B.: "Sopra i fenomeni di deformazione dei terreni da variazione della pressione di strato," Memorie Serie II, Atti della accademia della scienze della instituto di Bologna (1970) No. 6.
20. Eason, G. *et al.*: "On Certain Integrals of Lipschitz-Hankel Type Involving Products of Bessel Functions," *Phil. Trans.*, Royal Soc., London, **A 247**, 529.
21. Teeuw, D.: "Prediction of Formation Compaction from Laboratory Compressibility Data," *Soc. Pet. Eng. J.* (Sept., 1971) 263-271; *Trans.*, AIME, **251**.
22. Nair, K.: "Analytical Methods for Predicting Subsidence," *Land Subsidence*, Publication No. 69, AIHS-UNESCO (no date of issue) **2**, 588.
23. Sandhu, R. S. and Wilson, E. L.: "Finite Element Analysis of Land Subsidence," *Land Subsidence*, Publication No. 89, AIHS-UNESCO (no date of issue) **2**, 393.
24. Teeuw, D.: "Laboratory Measurements of Compaction Properties of Groningen Reservoir Rock," *Verhandelingen Koninklijk Nederlandsch Geologisch Mijnbowkundig Genootschap* (1973) **28**, 19.
25. Geertsma, J.: "A Theoretical Analysis of the Compaction-Subsidence Relationship: The Homogeneous Case," *Ibid.*, 43.
26. Geertsma, J. and van Opstal, G.: "A Numerical Technique for the Prediction of Subsidence Above Compacting Reservoirs, Based on the Concept of Nuclei of Strain," *Ibid.*, 63.
27. Van Kesteren, J.: "Prediction of Possible Future Subsidence Resulting from Gas Production in the Groningen Field," *Ibid*, 11.
28. Van Kesteren, J.: "Estimate of Compaction Data Representative of the Groningen Field," *Ibid.*, 33.
29. Newman, G. H.: "Pore Volume Compressibility of Reservoir Rocks Under Hydrostatic Loading," *J. Pet. Tech.* (Feb., 1973) 129-134.
30. Sawabini, C. T., Chilingar, C. T. and Allen, D. R.: "Triaxial Compaction of Unconsolidated Oil Sands," paper SPE 4058 presented at SPE-AIME 47th Annual Fall Meeting, San Antonio, Tex., Oct. 8-11, 1972.

JPT

Paper (SPE 3730) was presented at SPE-AIME European Spring Meeting, held in Amsterdam, May 16-18, 1972.